

3D 프린팅 공정을 이용한 고체 산화물 연료전지 연구 동향

주바이르 마사우드^{1,2*} · 무하마드 주바이르 칸^{3*} · 암자드 후세인^{1,2} · 하피즈 아흐마드 이시팍^{1,2} · 송락현^{1,2†} · 이승복^{1,2} · 조동우¹ · 임택형^{1,2}

¹한국에너지기술연구원 연료전지연구실, ²과학기술연합대학원대학교 에너지 및 시스템 공학 전공, ³굴람이샤크칸과학기술대학교 재료공학과

Recent Activities of Solid Oxide Fuel Cell Research in the 3D Printing Processes

ZUBAIR MASAUD^{1,2*}, MUHAMMAD ZUBAIR KHAN^{3*}, AMJAD HUSSAIN^{1,2}, HAFIZ AHMAD ISHFAQ^{1,2}, RAK-HYUN SONG^{1,2†}, SEUNG-BOK LEE^{1,2}, DONG WOO JOH¹, TAK-HYOUNG LIM^{1,2}

¹Fuel Cell Laboratory, Korea Institute of Energy Research, 152 Gajeong-ro, Yuseong-gu, Daejeon 34129, Korea

²Department of Advanced Energy and System Engineering, University of Science and Technology (UST), 217 Gajeong-ro, Yuseong-gu, Daejeon 34113, Korea

³Department of Materials Science and Engineering, Ghulam Ishaq Khan (GIK) Institute of Engineering Sciences and Technology, Tarbela Road, District Swabi, Khyber Pakhtoon Khwa, Topi, Swabi, Khyber Pakhtunkhwa 23640, Pakistan

†Corresponding author :

rhsong@kier.re.kr

*Both authors have contributed equally.

Received 5 January, 2021

Accepted 28 February, 2021

Abstract >> Solid oxide fuel cell (SOFC) has received significant attention recently because of its potential for the clean and efficient power generation. The current manufacturing processes for the SOFC components are somehow complex and expensive, therefore, new and innovative techniques are necessary to provide a great deal of cell performance and fabricability. Three-dimensional (3D) printing processes have the potential to provide a solution to all these problems. This study reviews the literature for manufacturing the SOFC components using 3D printing processes. The technical aspects for fabrication of SOFC components, 3D printing processes optimization and material characterizations are discussed. Comparison of the SOFC components fabricated by 3D printing to those manufactured by conventional ceramic processes is highlighted. Further advancements in the 3D printing of the SOFC components can be a step closer to the cost reduction and commercialization of this technology.

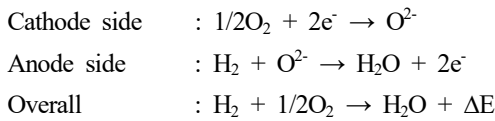
Key words : Solid oxide fuel cell(고체산화물 연료전지), 3D printing (3D 프린팅), Ceramics(세라믹), Manufacturing processes(제조공정)

1. Introduction

Solid oxide fuel cell (SOFC) is an electrochemical

device which converts the chemical energy from the hydrogen fuel to electrical energy^{1,2}. The working of the SOFC is illustrated in Fig. 1. The SOFC is com-

posed of three main components namely the anode, electrolyte, and cathode^{3,4}). The operation of the SOFC starts by supplying air and fuel to the cathode and anode, respectively⁵). At the cathode side, the oxygen after conversion to oxygen ions diffuses through the cathode, as it contains oxygen ion deficiencies, to the electrolyte⁶). The electrolyte is an ionic conductor that conducts those oxygen ions to the anode side where it reacts with the fuel to generate electrons⁷). The summary of the reactions in the SOFC is given next⁸).



The SOFC single cell can be structured into a vari-

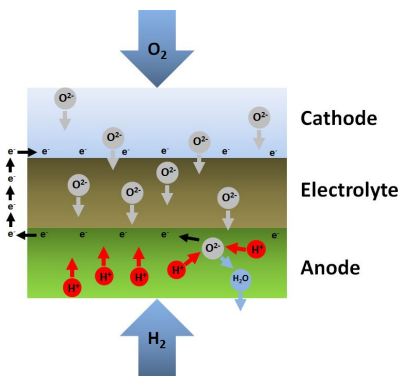


Fig. 1. Schematic illustration of the working principle of the SOFC

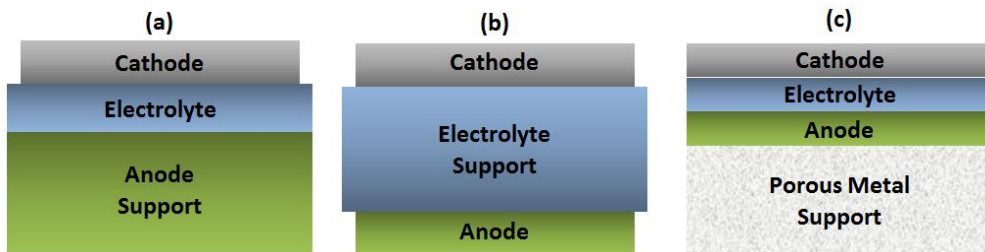


Fig. 2. Various types of SOFC configurations including (a) anode supported, (b) electrolyte supported, and (c) porous metal-supported type SOFC

ety of configurations dependent on the requirement. There are two broad categories into which the configurations can be classified i.e. the self-supporting and external-supporting⁹). The self-supporting configurations can be further divided into the anode supported (Fig. 2[a]) or electrolyte (Fig. 2[b]) depending on the component used as a support. In the self-supporting configuration, the support is one of the SOFC components whereas, in the external-supporting configuration, an external substrate other than the cell components is used as a support (such as porous metal support shown in Fig. 2[c])¹⁰).

The SOFC can also be fabricated in the form of different designs. Two of the most commercialized SOFC designs include the tubular and the planar design^{11,12}). The tubular design shown in Fig. 3(a) consists of a cell fabricated in the form of a tube. The tubular cells show higher mechanical and thermal stability and simpler gas seal requirements but offer lower power densities as compared to the planar cells¹³⁻¹⁵). On the other hand, planar cell design shown in Fig. 3(b) consists of components fabricated in the form of flat layers. The planar design is preferred because of its cost-effectiveness, simple design, high power density, and ease of fabrication^{16,17}). However, in the case of planar cells, it is difficult to achieve good sealing of the cell¹⁸). Moreover, another design known as the flat tubular design (Fig. 3[c]) combines all the advantages of planar and tubular designs and minimize the

limitations associated with those two designs¹⁹).

Several manufacturing techniques such as tape casting²⁰⁻²⁹, screen printing³⁰⁻³⁴, sputtering³³⁻³⁷, spray pyrolysis³⁸⁻⁴², physical vapor deposition (PVD)⁴³⁻⁴⁵, chemical vapor deposition (CVD)⁴⁶⁻⁵⁰, electrophoretic deposition (EPD)⁵¹⁻⁵³, inkjet printing^{54,55} etc. have been used in the fabrication of the SOFC components. The tape casting process is associated with limitations such as difficulty in producing layers less than 10 μm and lesser design flexibility⁵⁶. On the other hand, screen printing is usually a manual process and it is difficult to achieve uniformity through it⁵⁷. Processes such as PVD, CVD, and EPD are costly processes and require huge capital costs⁵⁷. Moreover, to produce a SOFC stack a very high number of steps (more than 100 steps) are required⁵⁸. This large number of steps compromise the reliability of the SOFC system because of the multiple joints and seal requirements to achieve the stack⁵⁷.

Many research works have been dedicated to the commercialization of the SOFCs⁵⁹⁻⁶². To commercialize the SOFC there is a need for a single-step fabrication technique that is not only cost-effective, automated, and simple in function but also provides design flexibility, reproducibility, durability whilst re-

sulting in high-performance cells⁵⁶. Three dimensional (3D) printing is a single step and automatic process which has the potential to overcome the limitations associated with the conventional manufacturing processes of the SOFCs. Implementation of the 3D printing processes would play a pivotal role in the production of highly durable and reproducible SOFCs. Moreover, by using the 3D printing processes, the initial startup cost and the fabrication cost can also be decreased. It also has the potential to increase the SOFC design flexibility whilst reducing the energy cost and the material wastage at the same time, In this context, pursuing the 3D printing processes would be a major step towards the commercialization of the SOFCs.

The present work reviews the 3D printing processes for the fabrication of the SOFC components and complete unit cell, material characterization, and 3D printed cell performance. This paper is divided into seven different sections. The first section i.e. three-dimensional printing (3D printing) reviews the 3D printing process, its various types, and process parameters in detail. The next four sections review the use of 3D printing for the manufacturing of the components of the SOFC i.e. electrolyte, anode, cath-

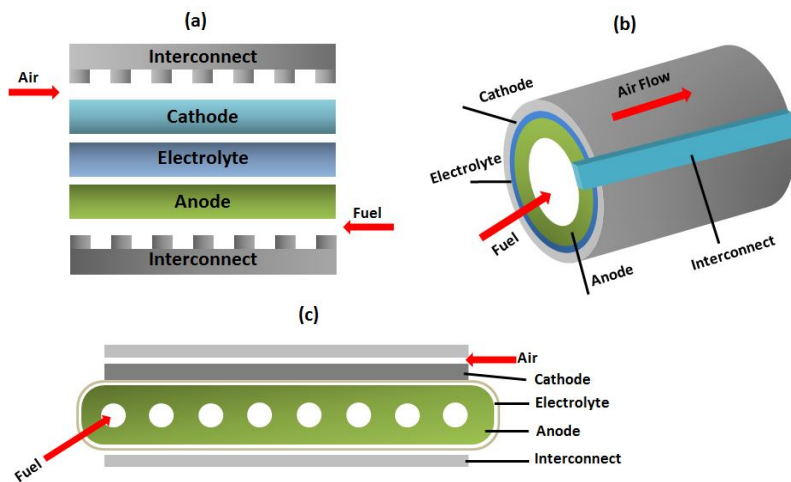


Fig. 3. SOFC geometries comprising of (a) planar, (b) tubular, and (c) flat-tubular SOFC geometries

ode, and manifold respectively. The section “complete single SOFC” focuses on the production of the complete 3D printed SOFCs. This paper is concluded by giving a summary and outlook towards the 3D printing of the SOFCs.

2. Three dimensional printing

2.1. Process and mechanism

3D printing is an additive manufacturing process in which the material is added layer upon layer to achieve the final product⁽⁶³⁾. The schematic of the 3D printing process is represented in Fig. 4. The 3D printing process begins by creating a model of the final product with the help of computer-aided design (CAD)⁽⁶⁴⁾. The model produced is then subjected to change in the STL (stereolithography) file format. The STL file format slices the model in layers to assist with the layer by layer deposition⁽⁶⁵⁾. After that, the STL file is uploaded to the printing machine where printing is performed in a layer by layer fashion to achieve the final product⁽⁶³⁾. It may be noted that after the production of the part by 3D printing, usually sintering is required to achieve the final strength of the fabricated part.

2.2. Characteristics of the 3D printing process

The 3D printing process carries numerous advan-

tages over the other subtractive technologies in terms of material wastage, cost, and automation. In contrast to other processes such as the injection molding and casting techniques, there is no need for expensive molds, tools, and dyes to be used⁽⁶⁶⁾. Additionally, no complex and labor-intensive machining is required for the part after manufacturing. Moreover, 3D printing is an automated process thus eliminating the element of human errors. The ability to recycle as much as 98% of the waste material makes it one of the most cost-effective technologies⁽⁶⁷⁾. The applications of 3D printing majorly lie in the production of prototypes, replacement parts, and medical/dental implants⁽⁶⁶⁾. However, the 3D printing process is also associated with some limitations such as it provides a reduced choice of materials, limited strength, and higher cost for producing a large number of products.

2.3. Types of 3D printing

2.3.1 Inkjet printing

Inkjet printing is a 3D printing technique that utilizes inks as a source of the required material and produces the required model with the help of layer by layer deposition⁽⁶⁸⁾. The advantages of the inkjet printing are 1) low cost⁽⁵⁶⁾; 2) high reproducibility⁽⁵⁶⁾; 3) low material wastage⁽⁶⁹⁾; 4) fine resolution control; and 5) simplicity⁽⁷⁰⁾. The inkjet printing mechanism is illustrated in Fig. 5.

The inkjet printing process also starts by creating

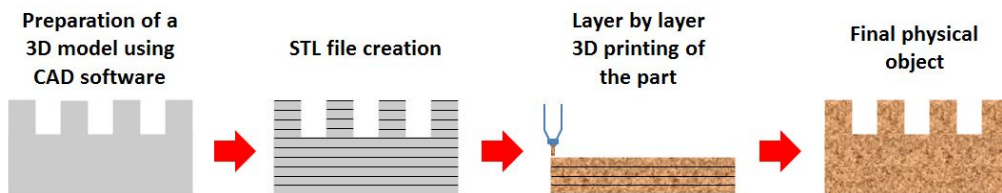


Fig. 4. Demonstration of the steps involved in the 3D printing process

a CAD model of the required part which is then converted to an STL file and uploaded to the printing machine⁷¹). The required ink containing a specific composition is prepared and the cartridge (ink reservoir) is filled with ink⁷⁰). The ink is then sent to the printing head where it reaches the nozzle and is printed on the substrate⁶⁸). After the deposition of the first layer, drying time is given for the solvent to dry or evaporate⁷²). The second layer is then deposited on the first and this procedure is repeated to achieve the final product⁷²).

2.3.1.1. Ink composition and properties

The inks used for inkjet printing of ceramics usually consists of these components⁷³): 1) powder of the material which is to be deposited, 2) a solvent which acts as a liquid carrier for carrying the powder particles, 3) a dispersant used to disperse the powder particles in the solvent and prevent agglomeration, and 4) a surfactant to prevent the nozzle from clogging⁷³).

For selection of the ink for the inkjet printing process, numerous properties of the 3D printing ink are to be considered including its surface tension, density, and viscosity⁷⁴). Jettability which is the ability to form a continuous flow after passing through the nozzle is affected by these properties⁷⁴). To assess the jettability of the material some dimensionless numbers are considered i.e. Reynolds (Re), Weber (We), and Ohnesorge (Oh) numbers⁷⁴). Re, We, and Oh numbers are the ratio of inertial forces to viscous forces (Eq. 1), the ratio of inertial forces to surface tension forces (Eq. 2), and the ratio of viscous forces to the surface tension and inertial forces (Eq. 3) respectively.

$$Re = \frac{\rho VL}{\eta} \tag{1}$$

$$We = \frac{\rho V^2 L}{\sigma} \tag{2}$$

$$Oh = \frac{\sqrt{We}}{Re} = \frac{\eta}{\sqrt{\rho L \sigma}} \tag{3}$$

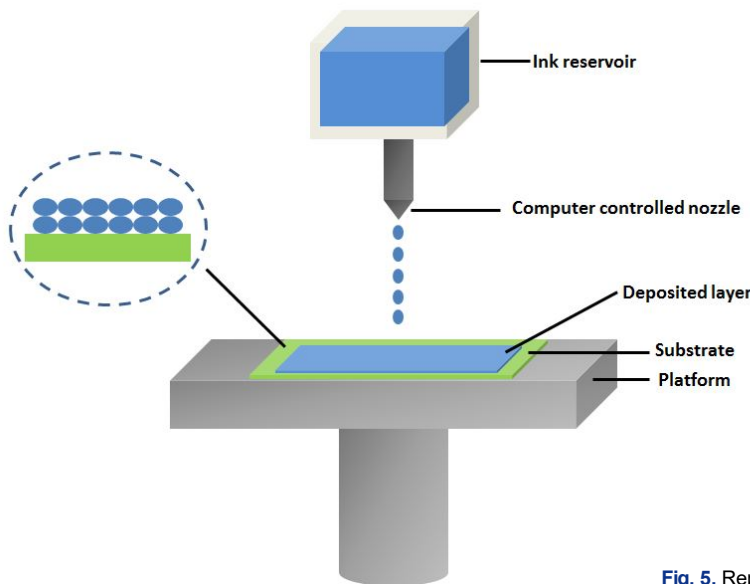


Fig. 5. Representation of the inkjet printing apparatus

In the above equations, ρ , η , σ , L , and V are the density, viscosity, surface tension, nozzle diameter, and droplet velocity, respectively. To achieve stable droplets of the ink, the value of Z , which is the reciprocal of the Oh number, should be larger than 2^{75} or at least in the range of $1 < Z < 10^{76}$.

2.3.2. Aerosol jet printing

Aerosol jet printing (AJP) is a method similar to inkjet printing but differs in a way that it uses aerosolized inks⁷⁷. The advantages of the AJP include 1) ease of patterning, 2) high reproducibility, and 3)

high resolution. The inks can be aerosolized pneumatically or by using the ultrasonic method⁷⁸. After the creation and uploading of the CAD model to the AJP machine, the aerosol stream flows towards the print head where a coaxial sheath gas flow focuses it aerodynamically onto the substrate to deposit the layer (Fig. 6)⁷⁸.

2.3.3. Fused deposition modeling

Fused deposition modeling (FDM) is an additive manufacturing process in which the raw material in the form of a filament feedstock is deposited layer by

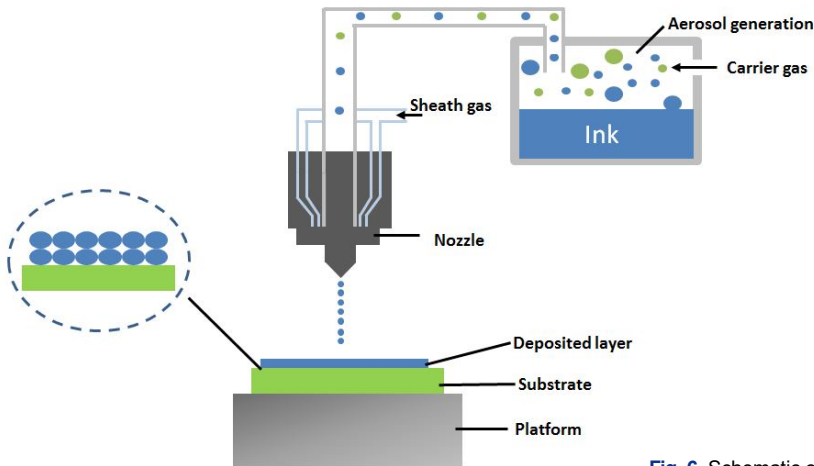


Fig. 6. Schematic of the aerosol jet printing (AJP) process

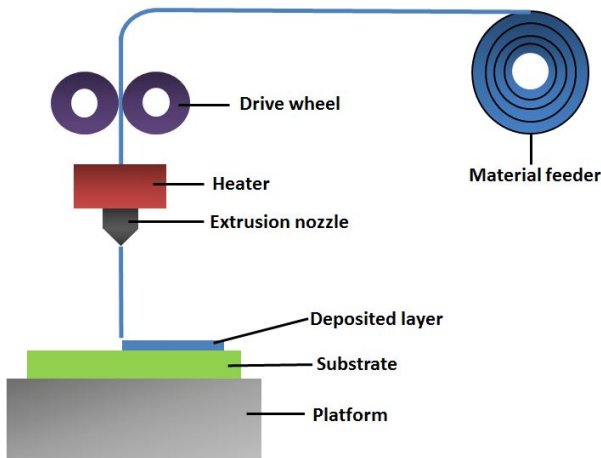


Fig. 7. Schematic representation of the FDM process

layer via extrusion, to achieve the required product⁶⁵. The FDM process is advantageous in a way that has 1) high reproducibility⁷⁹, 2) can produce complex geometries⁸⁰, and 3) produce parts safely in an office-friendly environment⁸⁰. To start the FDM process a CAD model is prepared and converted to an STL file, which is then uploaded to the FDM machine⁸¹. The schematic illustration of the FDM process is shown in Fig. 7.

The FDM system consists of a coil of the material, a liquefier head, an extrusion nozzle, and a build platform. The material to be deposited is supplied to the liquefier head in the form of a filament which is unwound from the coil⁸². Heating elements are incorporated within the liquefier head which converts the material into a semi-molten state⁸⁰. After that, the material is extruded from the extrusion nozzle that moves in the X-Y plane following the computer model. Moreover, when the first layer is deposited, the build support moves downwards for the deposition of the additional layers. In this way layer by layer deposition of the material is done to achieve the final product⁸¹.

2.3.4. Stereolithography

Stereolithography (SLA) is a 3D printing technique

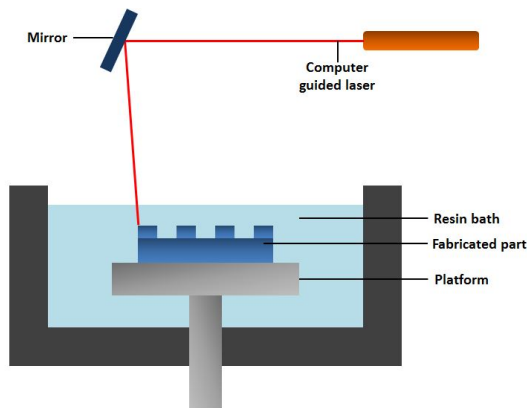


Fig. 8. Schematic illustration of the SLA apparatus

that relies on the photopolymerization of the resin or polymer to produce the required part^{83,84}. The advantages of SLA include: 1) can prepare fully-dense structural ceramics, 2) shows high resolution, and 3) excellent surface finish⁸⁵.

Like any other 3D printing process, the model of the required product is prepared on the CAD, followed by converted to the STL file and uploading it to the SLA machine⁸⁴. SLA process uses photo-curable resins (usually monomers) which are cured under the influence of a laser⁸⁶. As shown in Fig. 8, in the SLA system there is a resin tank with a support platform. The laser which is computer-controlled cures the resin according to the required pattern⁸⁷. As a result of curing, the resin solidifies and adheres to the support platform. Following the deposition of the first layer, the platform is removed and a layer of liquid resin is coated on the printed sample which is then subjected to curing⁸⁷. This procedure is repeated to achieve the required part.

2.3.5. Selective laser sintering

Selective laser sintering (SLS) is a 3D printing process in which a powder is sintered using a laser to achieve the final product⁸³. SLS provides advantages in many ways such as 1) construction of complex internal and external geometries, 2) no usage of

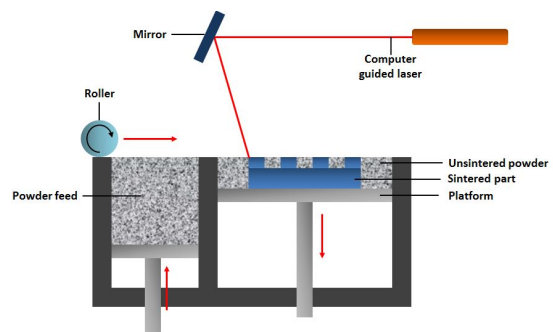


Fig. 9. Schematic illustration of the SLS process

organic solvents, 3) easier to incorporate multiple materials, 4) fast and cost-effective, and 5) any powder that fuse but not decompose under laser can be produced⁸⁸⁾.

After the preparation of the CAD model, the STL file is uploaded to the SLS machine. The SLS system shown in Fig. 9 contains a powder bed. The laser in the system is computer controlled and guides the laser movement according to the pattern required⁸⁸⁾. The energy from the laser is utilized to fuse and bind together the powder particles⁸⁹⁾. The binding between the powder particles can be achieved via solid-state sintering, liquid phase sintering, or sintering by full melting⁹⁰⁻⁹²⁾. After the first layer is formed the platform moves downwards and another layer of granules is added. The process is repeated to achieve the final product⁹³⁾.

3. Electrolyte

The electrolyte is a very critical component of the SOFC which requires being dense and thin. The dense electrolyte prevents the intermixing of fuel and oxidant, whereas, the thinner electrolytes are used to reduce the ohmic losses and the area-specific resist-

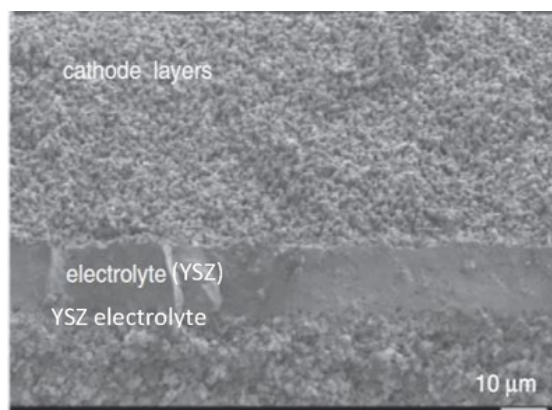


Fig. 10. shows the dense electrolyte fabricated via 3D printing. Printed with permission from [112]

ance of the cell⁹²⁻⁹⁴⁾. Therefore, the method of 3D printing used in the preparation of electrolyte should satisfy the aforementioned requirements of an electrolyte. Moreover, the cells in which the electrolyte is fabricated by the 3D printing processes should exhibit high electrochemical performance.

Inkjet printing and SLA are the most used 3D printing methods for the fabrication of thin-film SOFC electrolyte⁹⁴⁻¹¹⁰⁾ and stabilized zirconia is the mostly commercialized electrolyte material¹¹¹⁾. Most research on the 3D printing of the SOFCs has been focused on electrolyte fabrication.

The first major concern regarding the 3D printing processes is their ability to fabricate a dense electrolyte. Responding to that concern, many researchers in the reported work were able to manufacture dense SOFC electrolytes using 3D printing processes⁹⁴⁻¹¹⁰⁾. Fig. 10 shows the dense electrolyte fabricated via 3D printing processes.

Another crucial parameter is the thickness optimization of the electrolyte film. The electrolyte is generally preferred to be thin because a thicker electrolyte will lead to more performance losses due to the relatively poor ionic conductivity of it¹¹²⁾. Both inkjet printing and SLA are utilized for the fabrication of thin SOFC electrolytes. Farandos et al.¹⁰²⁾ fabricated a 23 μm YSZ electrolyte using inkjet printing. Inkjet printing was also utilized by Sukeshini et al.^{68,106)} to produce the YSZ electrolyte of thickness 10 μm . Tomov et al.⁶⁷⁾, Li et al.⁵⁴⁾ and Esposito et al.⁷⁰⁾ were able to manufacture YSZ via inkjet printing with thickness as low as 2 μm , 1.5 μm , and 1.2 μm respectively. Additionally, the GDC electrolyte of thicknesses 3 μm and 8 μm were also produced by El-Toni et al.¹⁰⁰⁾ and Wang et al.^{99,103)} respectively, by utilizing inkjet printing. Moreover, the technique of SLA was utilized by Masciandaro et al.¹¹⁰⁾ and Kirihara⁹⁵⁾ to produce YSZ electrolyte but

with thicknesses >10 μm. As a result of utilizing the 3D printing processes, the thin 3D printed electrolyte contributed towards the low ASR values in these works.

Another way of achieving high-quality inkjet printed YSZ film is by optimizing the printing parameters such as nozzle opening time, printing pressure, layer overlapping, the thickness of the printed layer, and the number of printing layers. Tomov et al.⁶⁷⁾ optimized all the printing parameters for printing a YSZ electrolyte via inkjet printing. They prepared various suspensions by varying the mass load of the YSZ powder in the range of 5-15%. However, the suspension with a 15 wt% mass load was chosen for optimizing procedure because its droplet showed more visibility on the substrate as compared to other compositions. Here, important factors to be considered are the roundness (R) and circularity (C) as shown in equations 4 and 5, respectively.

$$R = \frac{4A}{\pi a^2} \quad (4)$$

$$C = \frac{4\pi A}{p^2} \quad (5)$$

In equation 4 and 5, A is the area of the ellipse, a and b are the major and minor axes of the ellipse, and p is the perimeter. Image J analysis was used to analyze these values. Moreover, the values for R and C is 1 for a perfect circle⁶⁷⁾. Hence, the jet opening time of 500 μs and printing pressure of 0.8 kgcm⁻² were selected as the optimized condition for inkjet printing of the YSZ electrolyte as they depicted the highest R and C values.

The thickness of the printed layer is a key factor in the deposition of the electrolyte layer by inkjet printing. Regarding the thickness of the printed layer, the most important factor is the critical cracking

thickness (H_{crit})¹¹³⁾. The H_{crit} is defined as the thickness of the film at which the cracking of the film occurs. The dependency of various parameters on H_{crit} is shown in equation 6.

$$H_{crit} = R \cdot 0.050 \left(\frac{GN\Phi R}{2\pi(1-\nu)\gamma} \right)^{\frac{2}{3}} \quad (6)$$

where, R is the deposited particle radius, N the coordination number, Φ is the particle packing density, ν is the poisson ratio and γ is the surface area.

Ink composition plays a pivotal role in inkjet printing; an optimized ink can lead to better results and fewer defects. The ink is comprised of three components i.e. the solvent, the dispersant particles, and the functional oxide particles⁹⁹⁾. Out of the three, the solvent is the most crucial component as both the stability and rheological properties of the ink are affected by this⁹⁹⁾. For that purpose, Wang et al.⁹⁹⁾ optimized the GDC inks using a solvent incorporating α-terpineol and methanol mixture. Various inks were prepared by using different ratios of terpineol and methanol as shown in Table 1. A higher α-terpineol amount led to lower sedimentation and stable inks. However, with the increase in α-terpineol content the viscosity of the solvent also increased which hinders the drop ejection. Thus, the ink 55 in Table 1 was considered as the optimum ink as it satisfied all the criteria required

Table 1. Summary of the inks produced in ref. [99]

Type of ink	Jetting pressure (mbar)	Terpineol to methanol volume ratio	Viscosity (cP)
Inktm28	100	20:80	7.2
Inktm37	100	30:70	12.5
Inktm46	200	40:60	15.2
Inktm55	400	50:50	19.2
Inktm64	700	60:40	23.1
Inktm73	Not printable	70:30	25.6

such as ink stability, drop integrity, and printability. Moreover, using the optimized ink (ink 55), they also optimized the printing parameters for the GDC suspension. The nozzle opening times and printing pressure were optimized to be around 550-600 μs and 400-800 mbar respectively.

An additional factor affecting the printing of the electrolyte layer via inkjet printing is the concentration of the inks which was exploited by Esposito et al.⁷⁰⁾. In that work, two YSZ inks were prepared: a dilute ink (0.9 vol.% powder) and a concentrated ink (3.7 vol.% powder). It was found out that extremely dilute inks e.g. 0.9 vol. % (6 wt. %) ink can result in residual porosity and pinholes. However, the concentrated inks e.g. 3.7 vol. % (20 wt. %) led to better densification when multilayer printing was done and produced fewer pinholes.

Other than that, 3D printing provides immense advantages over other conventional techniques when it comes to complex designs and shapes. It has been reported that the corrugated design of the support could lead to higher performances¹¹⁴⁻¹¹⁶⁾. However, the limi-

tation of other techniques led to researchers not using those designs. Moreover, the electrolyte self-supported SOFCs have also been attracting attention due to the simplicity of stack design as shown in Fig. 11.

For that purpose, Xing et al.¹¹⁷⁾ and Masciandaro et al.¹¹⁰⁾ manufactured YSZ electrolyte self supports using the 3D printing processes. Moreover, Pesce et al.¹¹⁴⁾ developed YSZ corrugated electrolyte support by using the 3D printing process of SLA. The corrugated supports outperformed the traditional electrolyte support with an increase of 57% in performance. Similarly, Xing et al.¹¹⁸⁾ manufactured a ripple shaped electrolyte with Digital light processing (DLP)-SLA process. The ripple shaped electrolyte showed a 32% increase in the performance as compared to the flat cells. 3D printed electrolytes showed good electrochemical performances in various other studies which are summarized in Table 2^{54,67,68,70,98,102,106,110,114,119,120)}. In these reference studies, an electrolyte in the unit cell was fabricated using 3D printing processes.

To sum up this section, it can be safely concluded that 3D printing processes such as inkjet printing and

(a) Tape Casting Route



(b) Extrusion Route



(c) 3D- Printing Route



Fig. 11. The design simplicity offered by 3D printing (c) over the other techniques (a, b)

SLA can be used for the fabrication of the SOFC electrolyte. The 3D printing processes provides numerous advantages over the other conventional techniques. The most important of which is the formation of complex designs such as the corrugated and ripple designs of the electrolyte support which ultimately led to an increase in the cell performances. Moreover, the development of the SOFC assembly using 3D printed self-supported electrolytes and then 3D printing of the assembly (Fig. 11) will lead to a humongous reduction in the number of steps required for the assembly and stacking of the SOFC which could be a huge step to the commercialization of the SOFCs.

The inkjet printing is reported to be the most feasible technique for the manufacturing of the electrolyte as most of the printing parameters for the inkjet printing of the electrolytes such as YSZ and GDC have been optimized. Moreover, the cells using inkjet-printed electrolyte has delivered high-performance results with peak power densities as high as 1.5 Wcm⁻² (Table 3). However, the fabrication of the electrolyte by SLA shows a lot of promise regarding the manufacturing of complex designs. Moreover, us-

ing the DLP-SLA process the speed of the manufacturing process could also be increased.

4. Anode

The anode is another major component of the SOFC. The anode of the SOFC requires stability at high temperatures¹¹²⁾, good electronic conduction¹²¹⁾, optimum porosity (optimized microstructure)⁸⁾, etc. Moreover, for the commercial applications, the anode should be easy to fabricate, fuel-flexible, and exhibit low cost¹²¹⁾.

The anode microstructure is of tremendous im-

Table 3. Different conditions of the cells fabricated in ref. [105] including the number of printing passes, sintering temperature, and peak power densities.

	Cell 1	Cell 2	Cell 3	Cell 4
Cathode	LSM	LSM	LSM	LSM
No. of printing passes	40	60	40	40
Sintering T (°C)	1,200	1,200	1,200	1,150
Solid wt. %	34.7	34.7	17.3	34.7
Peak Power Density at 800°C (Wcm ⁻²)	0.21	0.13	0.27	0.32

Table 2. Cell outputs of SOFC in which electrolyte was made via 3D printing

Printing method	Material used	Thickness (μm)	Open current voltage (OCV) (V)	Peak power density (PPD) (Wcm ⁻²)	Temperature (°C)	Reference
Inkjet	YSZ	1.2	1.15	1.5	800	[70]
Inkjet	YSZ	23	0.84	-	800	[102]
Inkjet	YSZ	10	1.14	0.30	800	[68]
Inkjet	YSZ	6	0.9	0.17	800	[98]
Inkjet	YSZ	5.9	1.01	0.17	800	[67]
Inkjet	YSZ	7.5	1.1	1.04	750	[54]
Inkjet	YSZ	10	1.14	0.46	850	[106]
SLA	YSZ	270	1.10	0.41	900	[114]
SLA	YSZ	340	1.14	0.1	900	[110]
DLP-SLA	YSZ	500	1.08	0.176	850	[119]
3D printing	SDC	1200	1.0	0.448	550	[120]

portance; an optimized microstructure can lead to higher performance cells. To improve the anode performance and reduce the polarization losses, infiltration has proven to be an effective method that increases the triple-phase boundaries (TPB)¹²². In recent years, many researchers have made efforts for the microstructural optimization of the anode using infiltration¹²³⁻¹²⁹.

One of the major problems regarding SOFCs is its high operation temperature¹³⁰. To resolve this issue anode component of the SOFC was used as the support to provide mechanical strength to the SOFC. Moreover, utilizing the anode as the support was a major development in lowering the temperature of the SOFCs^{131,132}. However, controlling the microstructure of the anode support is critical. The particle size, particle size distribution, porosity, size of the pores, and tortuosity remain the critical parameters to be addressed. Using other conventional techniques such as powder pressing, tape casting, etc, the control on these parameters is very difficult which results in problems relating to the reproducibility and ultimately the fuel cell performance. However, using an automatic process such as the 3D printing processes can lead to control over all the above-mentioned parameters and thus resulting in high power IT and LT SOFCs^{133,134}. For that purpose, Miyamoto et al.¹³³ developed Ni-YSZ supports using the SLA process. However, their work only was limited to the manufacturing of the supports and not the full cells. In this regard, the work of Han et al.¹³⁴ was very crucial. Not only did they develop the NiO-YSZ supports using the 3D printing process but also they fabricated the complete SOFC using the inkjet printing process. Development of the anode support by a cost-effective process such as inkjet printing is a major breakthrough and the advantages of high control over the microstructure such also be taken into consideration.

As far as the thin anode layers are concerned, Wang et al.¹³⁵ infiltrated GDC ink (1.5 M total metal concentration) using inkjet printing in the NiO-GDC scaffold. In this study, two types of cells were prepared. In the first type, the NiO-8YSZ anode support was prepared by the tape casting process and then pre-sintering was performed at 1,100°C. After that, the functional layer of NiO-GDC was inkjet printed on it and the cell was fired at 900°C to produce a porous NiO-GDC anode scaffold. After the infiltration, the GDC electrolyte was inkjet printed on the anode, and sintering was done at 1,400°C. Moreover, an $\text{La}_{0.6}\text{Sr}_{0.4}\text{Co}_{0.2}\text{Fe}_{0.8}\text{O}_{3-\delta}$ (LSCF) - $\text{Ce}_{0.9}\text{Gd}_{0.1}\text{O}_{1.95}$ (GDC) interlayer was screen printed on the anode followed by the addition of the current collection layer of LSCF by the same method. The complete cell was finally sintered at 1,200°C. However, the only difference in the other cell was that no infiltration was performed in it. It was referred to as the reference cell. The impregnation of GDC nanoparticles (size varying from 50-200 nm) led to an increased amount of TPB which resulted in higher electrochemical performance. Utilizing the multiple infiltrations i.e. 12 infiltration cycles, the performance was increased even further. The OCV and PPD (0.90 V, 380 mWcm^{-2}) of the infiltrated cell was higher as compared to the OCV and

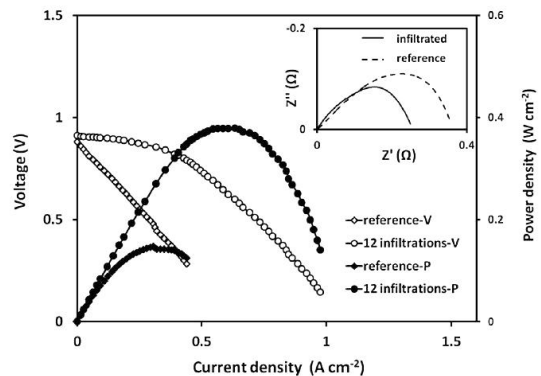


Fig. 12. I-V curve of an inkjet-infiltrated and reference cell. Reproduced from ref. [135]

PPD of reference electrode (0.85 V, 150 mWcm⁻²) at 600°C (Fig. 12). This implied a huge promotion factor of $\epsilon_{PPD}=2.53$ (where $\epsilon_{PPD}=\text{PPD}_{\text{inf}}/\text{PPD}_{\text{ref}}$).

Similarly, Mitchell-Williams et al.¹³⁶ infiltrated propionic acid-based and water based GDC inks utilizing the inkjet printing process in the NiO-8YSZ anode. Mitchell-Williams et al.¹³⁶ reported 7 and 12% higher power density at lower voltages for H₂O and PPA samples respectively when compared to the reference (un-infiltrated) cell. Moreover, the infiltrated cells displayed no substantial degradation after aging for 50 hours at 600°C as shown in Fig. 13.

Optimizing the printing conditions of the anode is another way to improve the performance of the SOFC anode. Therefore, Tomov et al.¹⁰⁴ optimized the printing conditions of a NiO-GDC anode. For that purpose, two suspensions were prepared, one in methanol (MeOH based inks) solvent and the other in 1-Propanol (PrOH based inks). The inks were deposited using direct ceramic inkjet printing (DCIJP) which is an influential technique for the fabrication of ceramic coatings. It is a non-contact method which can dispense droplets in the range of nL volumes¹⁰⁴. The anode was inkjet printed on a stainless steel porous support. To find out the optimum conditions, the temperature of the porous support was varied from

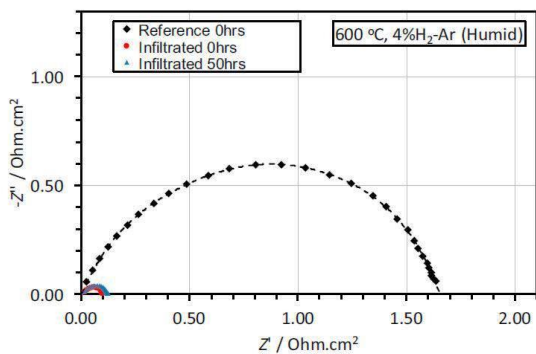


Fig. 13. Nyquist plot for GDC infiltrated NiO-8YSZ anode 0h aged, 50h aged, and reference cell (0h aged). Reproduced from ref. [136]

100-180°C and different opening times were provided to form a droplet on the substrate. As suggested by equations 4 and 5, to achieve high values of circularity and roundness, 120°C temperature and 400 μs opening time were chosen for the methanol solvent ink (Fig. 14[a]) whereas for the PrOH solvent temperature of 160°C and 500 μs were considered ideal (Fig. 14[b]).

To solve another major problem regarding anode of the SOFC i.e. the sulfur poisoning and carbon deposition in the direct carbon solid oxide fuel cell (DCFC), Dudek et al.¹⁰¹ used inkjet printed Ni-YSZ anode infiltrated with 0.5 M solution of Cu(NiO₃)₂·3H₂O in their study. This type of anode that is inkjet printed in this case, not only prevented sulfur poisoning, corrosion, and carbon deposition but also exhibited better electronic conductivity. Moreover, these cells with infiltrated Cu solution, exhibited an increased performance of 80 mWcm⁻² at 850°C as compared to 60 mWcm⁻² shown by the cell in which Cu was not infiltrated.

For the improvement in the electrochemical performance of the anode functional layer, AJP can be utilized. The AJP can be incorporated with a dual atomizer i.e. one for each component⁵⁵. In the dual

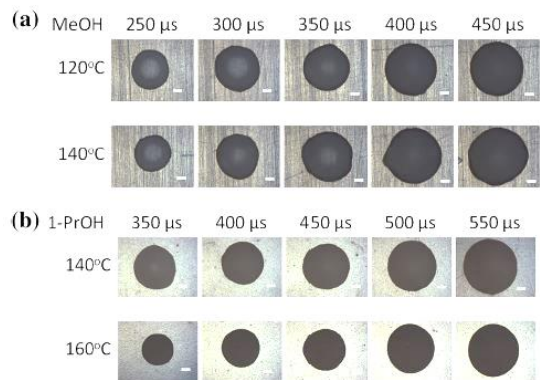


Fig. 14. Images of the drops at different substrate temperatures and opening times, (a) MeOH (methanol), and (b) PrOH based inks. Reproduced from ref. [104]

atomizer configuration, there are two separate chambers for two components. It allows the functional gradation of layer composition which provides the potential for improved cell design and higher performance⁵⁵⁾. Sukeshini et al.⁵⁵⁾ fabricated such functionally graded AFL by utilizing the dual configuration of the AJP composed of NiO/YSZ (type 2 cell) utilizing AJP on a tape cast anode support and compared its performance with the cell in which the AFL layer was not graded (type 1 cell), as displayed in Fig. 15. The microstructural analysis of both cells showed that the cell with functionally graded AFL showed a higher volume fraction of YSZ as compared to NiO in areas near the electrolyte when contrasted to the regions adjacent to the anode support thus resulting in higher performance than the non-graded cell.

The reported research work indicates that it is feasible to produce anode with the help of inkjet printing. The most important factor for improving the performance of the anode was the infiltration by using the inkjet printing machine. With the help of inkjet, printing excellent volume control, dosage, and distribution of the infiltrated particles can be achieved. By using DCIJP, even better results can be obtained as it spreads the droplets in nL volumes. With the help of AJP, gradation in the functional layer can be

achieved which can further increase the electrochemical performance. There have been reported works on 3D printing of anode support, which shows the immense promise of the 3D printing processes in the development of the anode supports. However, SLA is considered to be an expensive and slow process. So, the cost analysis of such a technique for the manufacturing of the anode support of SOFC would be a crucial development. Moreover, using inkjet printing for the development of the anode support was a crucial breakthrough. However, other 3D printing processes such as the FDM also need to be explored as a contender to the development of the anode supports of SOFCs. The work on the manufacturing of anode support of SOFCs using the 3D printing process is still in its early stages and needs more R&D in contribution to the high-performance SOFCs.

5. Cathode

The cathode is another core component of the SOFC. To achieve a high performance of the cell, the cathode must possess 1) optimum porosity for the diffusion of the oxygen; 2) stability under oxidation atmosphere; 3) high electronic and ionic conductivity;

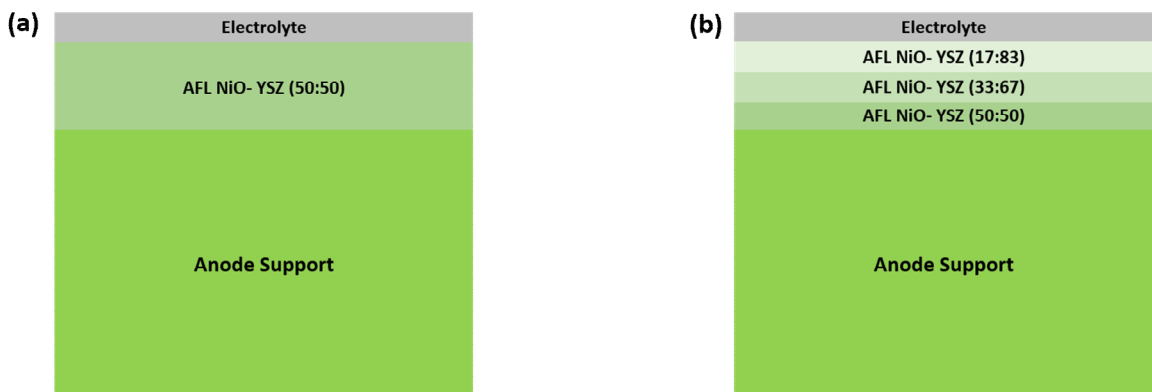


Fig. 15. Schematic of AFL; (a) nongraded and (b) graded fabricated in ref. [55]

and 4) low cost¹³⁷). Thus, the 3D printing process should fabricate a cathode exhibiting these properties.

Infiltration is an important technique by which the microstructure of the cathode can be improved. The infiltration results in an increase of the TPBs which result in smaller resistance values, consequently, resulting in higher electrochemical performance^{138,139}. The methods used for infiltration are usually micro-pipettes, syringes, or dip coating^{140,141}. These are manual techniques and reproducibility is a major issue associated with them¹⁴². However, Da'as et al.¹⁴² showed that as compared to other techniques, with the help of inkjet printing, controllable infiltration can be performed.

Similarly, Tomov et al.¹⁴³ infiltrated LSCF-GDC composite cathode scaffolds with ethanol-based $Ce_{0.9}Gd_{0.1}(NO_3)_3$ inks via inkjet printing under optimized conditions of 400 mbar pressure and 220 μ s opening time. Two types of cathodes i.e. LSCF: GDC 40:60 vol.% and LSCF: GDC 60:40 vol.% (denoted for further reference as 40:60 and 60:40 cathodes, respectively) were used in this study. Both types of cathodes (40:60 and 60:40) were infiltrated with the GDC ink. For reference, un-infiltrated samples with the same composition of the cathode were also prepared. In comparison with the as-sintered (un-infiltrated) cathode (Fig. 16[a]), the infiltrated cathodes

(Fig. 16[b]) showed lower resistances¹⁴². It may also be noted that the 60:40 cathodes showed more improvement in the polarization losses when infiltrated as compared to the 40:60 cathode. It was because the LSCF grains in the 60:40 electrode provided a higher grain surface availability for the nano-decoration with GDC nano-particles than the 40:60 electrode, thus extending the TPBs and also increasing the sites for oxygen reduction reaction (ORR). Hence, by infiltration and manipulating the ratio of two powders used in the composite cathode, the polarization losses in the cathode can be reduced resulting in higher electrochemical performance.

In the case of inkjet printing, for the optimization of cathode microstructure, optimization of ink parameters such as We and Z number becomes necessary. Fig. 17 illustrates the formation of defects in the un-optimized inks as compared to a defect-free optimized ink.

For that purpose, Hill et al.¹⁴⁴ prepared numerous α -terpineol based inks including 1) neat α -terpineol, 2) α -terpineol+ethyl cellulose (EC) (0.03-0.4 wt.%), 3) α -terpineol+ $La_{0.6}Sr_{0.4}Fe_{0.8}Co_{0.2}O_3$ (LSCF) (3.5-12 wt.%), and 4) α -terpineol+LSCF (3.5-12wt. %) + EC (0.03-0.4 wt. %). The inks were printed on YSZ electrolyte and glass substrates. In this work, the contributions of the Z and We numbers were distinguished

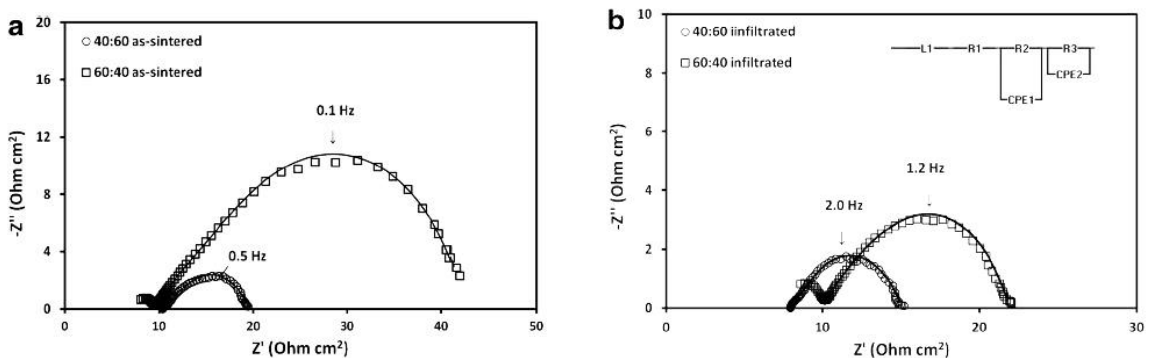


Fig. 16. Nyquist plot of (a) as-sintered and (b) infiltrated LSCF: GDC cathode. Reproduced from ref. [143]

by varying the droplet velocity or print-head temperature as it resulted in a change in those numbers e.g. at a velocity of 9 m/s, We number of 57 is achieved. In this work, it was explained that the We number is the crucial factor related to defect formation. Moreover, it was concluded that within the limit of Z number i.e. $3 < Z < 24$ there exists a threshold for We number i.e. 35 (Fig. 18). Printing above this threshold limit will result in defects such as splash and satellite defects as whereas printing below this threshold limit will result in uniform and defect-free droplets.

In an additional study by Han et al.⁷¹⁾, LSCF cathodes were fabricated by using a low-cost inkjet printer to achieve high cell performance. Different cathode samples with various printing cycles such as 40, 80, 160, and 200 were prepared and they were designated as L-50, L-100, L-150, and L-200 samples respectively. The L-50 and L-100 samples showed an inhomogeneous surface with cracks at various places in the samples. This can be attributed to the high thickness per printing cycle which resulting in slow

evaporation thus the cracks appeared at the surface. In the L-150 and L-200 samples, the microstructure improved as no cracks were observed on the surface. However, it should be noted that the L-200 sample resulted in a reduced amount of porosity which is not ideal for cathode microstructure. Therefore, a sample L-150 was considered ideal to achieve an ideal cathodic microstructure. The L-150 sample also resulted in the highest performance amongst other cathode performance with a power density of 377 mW cm^{-2} at 600°C ⁷¹⁾.

The electrochemical performance can also be improved by manipulation of the number of printing passes and the sintering temperature of the cathode. To exploit this effect, Sukeshini et al.¹⁰⁵⁾ utilized AJP to fabricate inkjet printed LSM cathode with LSM-YSZ interlayer. In this study, AJP was utilized to remove the need for ball milling of the two powders used in the composite cathode. The anode support in these cells was Ni-YSZ prepared from tape casting whereas the YSZ electrolyte was also printed

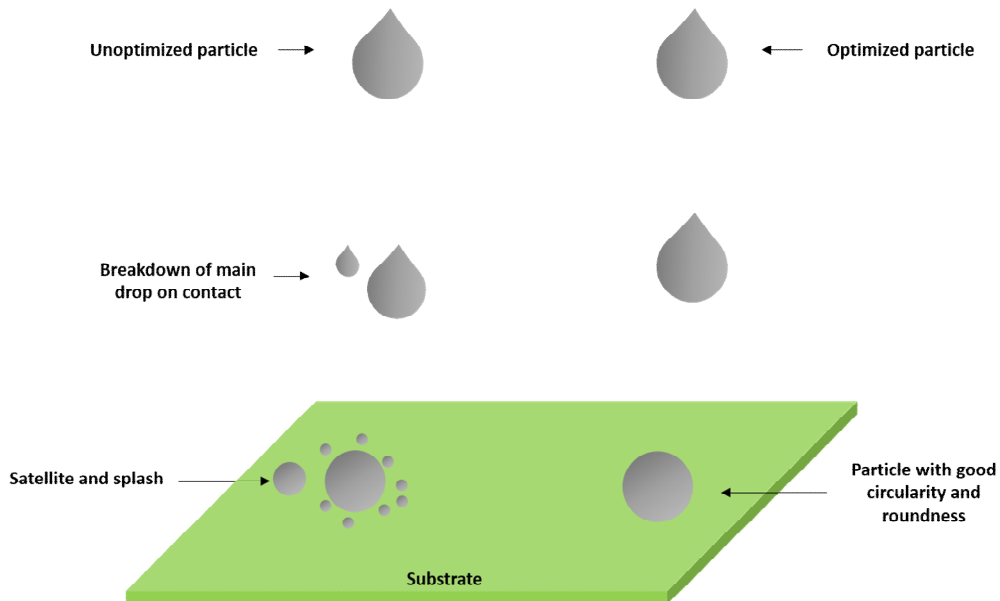


Fig. 17. Illustration of the formation of a defect-free droplet and a defected droplet using inkjet printing

using AJP¹⁰⁵). Four different types of cells were prepared by varying the number of printing passes, solids wt. %, and sintering temperature. The cell-1 comprised 40 printing passes, 1,200°C sintering temperature, and a solid wt.% of 34.7. Cell-2 had similar conditions to cell-1 except that it is comprised of 60 printing passes. Cell-3 although exhibited a similar sintering temperature and printing passes to cell-1 but comprised of 17.3 solids wt.%. However, the cell-4 had a different sintering temperature than the cell-1

(1,150°C) whereas the remaining conditions were similar to cell-1. Cell-4 exhibited the highest PPD as shown in the Table 3 which is made from the results obtained from this work. This was also suggested that further manipulation of these factors can result in further improvement of the performance. Moreover, by utilizing LSCF-GDC cathode the performance was increased twice as compared to that of LSM cathodes.

Moreover, to improve the cathode performance, inkjet printed composite cathodes are preferred as compared to the inkjet-printed single component cathode. Lee et al.¹⁴⁵) reported that the performance of an inkjet-printed composite cathode is higher than an inkjet-printed single component cathode. In this effort, it was observed that the inkjet-printed Ag-SDC cathode showed a superior performance to the inkjet-printed Ag cathode. The composite cathode showed a higher current density, power density, and a lower value of polarization losses as compared to the single component cathode. Accordingly, to achieve higher electrochemical performance, composite inkjet-printed electrodes are to be considered.

Additionally, to further improve the performance of the cathode Li et al.¹⁴⁶) used a pore former where

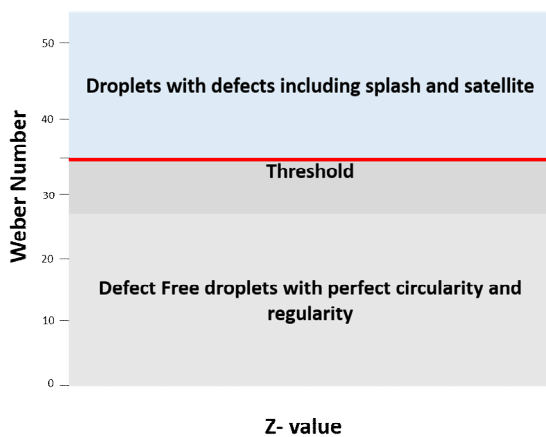


Fig. 18. Representation of the printing regions according to the We and Z numbers

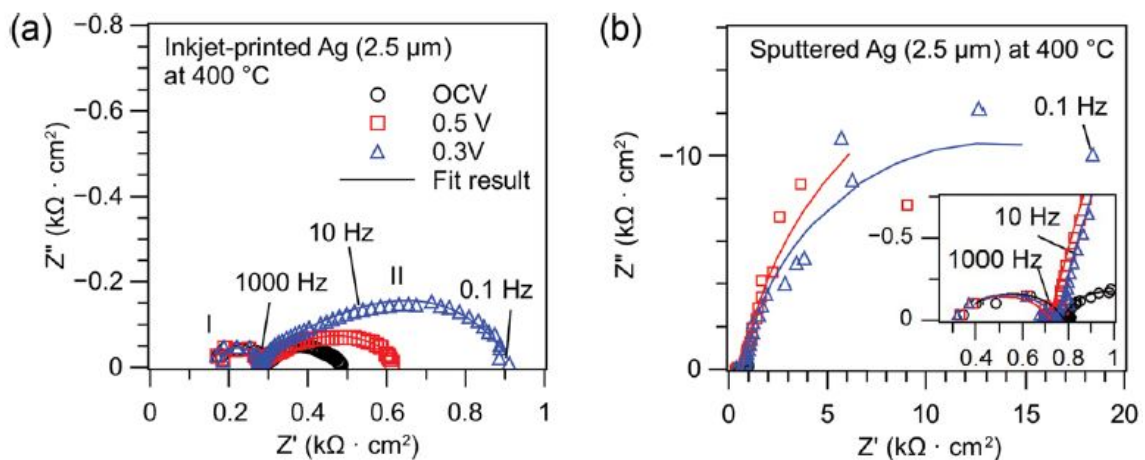


Fig. 19. Nyquist plots of (a) inkjet-printed and (b) sputtered Ag. Reproduced from ref. [147]

the pivotal role of pore former in the cathode was explained. For that purpose, a $\text{Sm}_{0.5}\text{Sr}_{0.5}\text{CoO}_3$ (SSC)+ $\text{Sm}_{0.2}\text{Ce}_{0.8}\text{O}_{1.9}$ (SDC) composite cathode was inkjet printed on a cell which is composed of NiO-YSZ anode support prepared by tape casting whereas the YSZ electrolyte and SDC buffer layer were prepared through the wet powder spraying technique. Three types of cathodes were inkjet printed. The electrode-1 had no pore former whereas the electrode-2 and electrode-3 comprised 15% and 10% PVP-K30 pore formers respectively. The electrode-3 showed the best results with high porosity, homogenous thickness, and good adherence to the buffer layer as compared to the other samples. The electrode-2 cells showed PPD as high as 940 mW cm^{-2} at 750°C .

Cathodes prepared by a 3D printing technique such as inkjet printing is advantageous over the other techniques in many ways. Yu et al.^[147] used Silver - $\text{Sm}_{0.2}\text{Ce}_{0.8}\text{O}_{1.9}$ (Ag-SDC) as a cathode material for LT-SOFC in which cathode was prepared via inkjet printing was compared to the cells prepared with the sputtering technique. The ASR values showed a clear difference between the inkjet-printed (Fig. 19[a]) and sputtered (Fig. 19[b]) samples. This was due to the

porous structure of the inkjet-printed cathode which provided more potential for the ORR, thus, leading to a lower ASR as compared to the sputtered cells which had a dense structure that contributed to a higher ASR value. Therefore, it can be seen in Fig. 20, that the cells in which inkjet printed cathode showed higher PPD and current density values than the sputtered cells. In these cells, platinum (Pt) was chosen as reference material for the cathode. It showed a higher performance because of its nano-porous structure which increases the ORR sites but it suffers severe degradation at elevated temperature^[140,141].

Moreover, it was also observed (in Fig. 21) that the inkjet-printed cathode remained porous even following the fuel cell test while the cathode which was subjected to sputtering displayed a dense microstructure with increased grain size^[147]. Hence, the inkjet printing is a more feasible way to deposit the porous Ag films as compared to the conventional sputtering technique^[147].

Sukeshini et al.^[106] compared the electrochemical performance of an inkjet-printed cathode to the screen-printed cathode. The cathode layers deposited for both types of cells were LSM-YSZ and LSM.

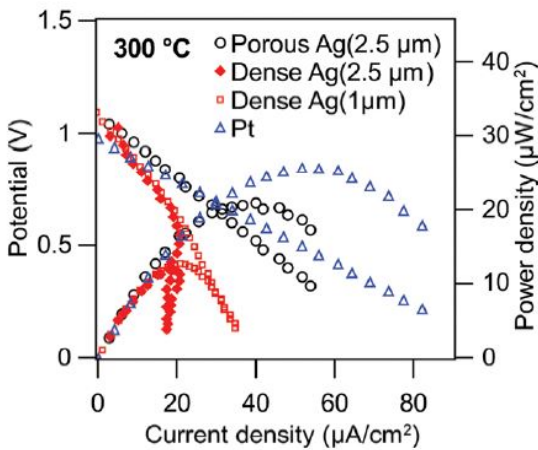


Fig. 20. I-V curve of inkjet printed porous Ag (2.5 μm), sputtered Ag (2.5 μm and 1 μm), and Pt. Reproduced from ref. [147]

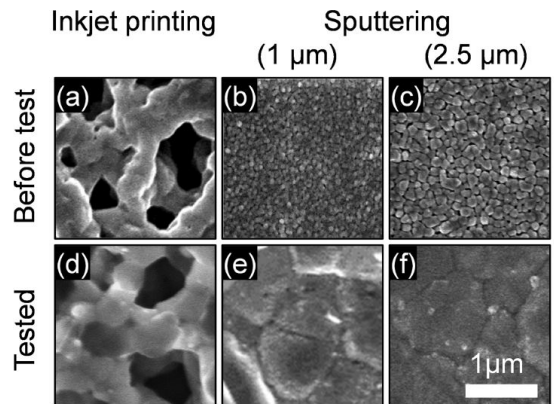


Fig. 21. SEM images of the inkjet-printed and sputtered samples before and after electrochemical testing. Reproduced from ref. [147]

Moreover, both the cells had a NiO-YSZ tape cast anode support whereas the anode interlayer (NiO-YSZ) and the electrolyte layers (YSZ) were deposited by the inkjet printing process. It was observed that the cells with inkjet-printed cathode showed almost identical performance to the cell with a slurry pasted cathode i.e. the PPD at 850°C was around 0.45mW cm⁻² for both types of cells.

Similarly, Yashiro et al.¹⁴⁸⁾ have also compared the inkjet printed and paste painted cathodes. Table 4 shows the three types of cells used in this study which are comprised of the same anode (NiO-GDC), electrolyte (GDC), and a cathode (LSCF-GDC). The cell-1 had a single layer inkjet printed cathode with a thickness of 3 μm. The cell-2 had a single layer of the painted cathode with 30 μm thickness. However, the cell-3 had a double layer (painted and printed) cathode with a thickness of 32 μm. In this work, TPBs created at the interface of the cathode particle, electrolyte, and oxidant gas phase is of major importance. With the increase in the TPBs, the ORR is increased which resulted in better electrochemical performance. It was observed that the cell-3 showed superior performance than the other two types of cells. This was because the inkjet printing increases the amount of TPBs formed thus increasing the performance. In the case of cell-1 (inkjet printed) at sintering temperature of 1,000°C a dense layer was produced which resulted in reduced performance of the cell. Cell-2 showed a higher performance than cell-2 because no

dense layer was observed for it. Cell-3 showed the highest performance as compared to the other two cells. This was because the inkjet-printed layer created a higher number of TPBs thus, contributing to higher electrochemical performance. Unlike cell-1, the inkjet-printed layer was covered by a painted layer which prevented it from becoming dense.

To produce high electrochemical performance using inkjet-printed cathode, Li et al.⁵⁴⁾ fabricated an SDC buffering layer by inkjet printed, deposited onto an inkjet-printed YSZ which was deposited on a NiO-YSZ tape cast anode support. The cells with SDC buffer layer and BSCF (also inkjet printed) as a cathode showed superior performance to the LSM cathode sample. Moreover, the SDC buffer layer BSCF cathode sample showed a PPD of 1,040 mW cm⁻² at 750°C which is very high when compared with that of an LSM cathode sample i.e. 600 mW cm⁻² at 750°C.

It can be concluded considering the reported work on the fabrication of cathode by 3D printing processes that inkjet printing is a feasible method for the production of it. Like the anode, infiltration in the case of the cathode has also proven to be an effective method to improve the performance of the cells having inkjet printed cathode. Moreover, by the optimization of the inkjet printing parameters and sintering temperature, the performance can be improved further improved. The inkjet printing for the cathode provided many advantages such as 1) automation, 2)

Table 4. Different planar cells fabricated having the same anode and electrolyte but different cathode. Cell 1 had an IJP cathode, cell 2 was fabricated using a painted cathode, whereas cell 3 comprised of a combination of painted and IJP cathode in ref [148].

	Cell 1	Cell 2	Cell 3
Cathode	LSCF-GDC	LSCF-GDC	LSCF-GDC
Printing type	Inkjet printing	Brush painting	First layer brush painting and second layer inkjet printing
Anode	NiO-GDC	NiO-GDC	NiO-GDC
Electrolyte	GDC	GDC	GDC

control of the film pattern, such as the size and thickness 3) high production reproducibility, 4) non-contact fabrication, and 5) additive fabrication. Additionally, it was shown in the reported work that the cells having inkjet printed cathode performed better than cells prepared using the sputtering and paste painting techniques, achieving performances with a peak power density as high as 1.04 Wcm^{-2} (Table 5). However, other than inkjet printing and AJP there has been no reported technique used for the fabrication of SOFC cathode.

5. Complete single SOFC

Developing a complete single SOFC with a single process is an immense task. Additive manufacturing provides a massive advantage that in this process no

destruction of material occurs (machining or other material removal processes) rather all the materials additively form the required product⁶¹⁾. Therefore, producing a complete SOFC from some 3D printing process will produce a low-cost SOFC which will help in the commercialization of it.

Sukeshini et al.⁶⁸⁾ in his earlier work developed all the non-supported layers i.e. the anode interlayer (NiO-YSZ), electrolyte (YSZ), cathode interlayer (LSM-YSZ), and cathode current collection layer (LSM) by inkjet printing process on NiO-YSZ anode support that was pre-sintered after being manufactured through the tape casting process. That cell was compared with another cell in which the cathode was painted while all the other layers were similar to the previous cell⁶⁸⁾. The results, in this case, indicated a higher performance for the pasted cathode cell i.e.

Table 5. The PPD of SOFC in which the cathode or buffer layer was fabricated from the 3D printing process

Printing method	Material used for cathode/ buffer layer	Peak power density (mWcm^{-2})	Temperature ($^{\circ}\text{C}$)	Reference
Inkjet	SDC (buffer)	1,040	750	[54]
Inkjet	SDC-SSC	940	750	[146]
Inkjet	LSCF-GDC	710	600	[148]
Inkjet	GDC-LSCF	600	800	[55]
Inkjet	LSM	460	850	[106]
Inkjet	LSCF	377	600	[71]

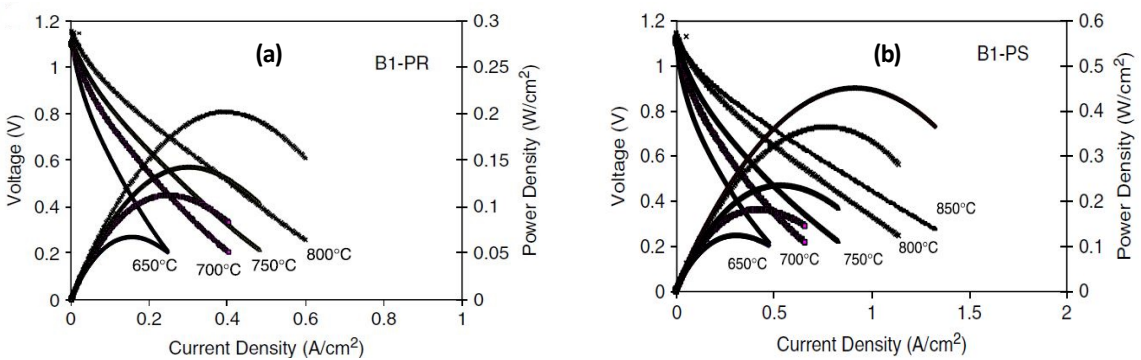


Fig. 22. I-V curves of (a) printed cathode and (b) pasted cathode. Reproduced from ref. [68]

0.38 W cm⁻² at 800°C as compared to the 0.21 W cm⁻² at 800°C of the printed cathode cell (Fig. 22). There was a clear difference in the performance values of the printed and pasted cathode cells. This was associated with the un-optimized inks used for cathode printing⁶⁸⁾.

For the further improvement of the previous work, Sukeshini et al.¹⁰⁶⁾ again dedicated a study to the manufacturing of a complete SOFC cell. The same types of cells were prepared as used in the previous study⁶⁸⁾. However, in this work, they changed the solid loadings in the cathode ink to optimize the inkjet-printed cathode layer of LSM. The solid loading was increased from 0.5 vol. % (used in ref. [68]) to 4 vol. % which led to the cathode ink optimization. The electrochemical performance of the two types of cells was compared again. These optimized cells showed an identical performance to the pasted cathode cell was observed i.e. 0.46W cm² at 850°C for

both the cells. Moreover, the impedance plot suggested that the impedance values for the printed cathode were lower as compared to the pasted cathode thus indicating a good potential for the inkjet printing process in the manufacturing of a complete SOFC. This displayed that inkjet printing is a better alternative to screen printing or pasting as the cells fabricated by inkjet printing not only showed a similar performance but also presented lower ASR values.

Moreover, Manogharan et al.⁹⁷⁾ introduced a novel 3D fabrication process known as binder jetting and produced a complete SOFC using this technique. In this process, a layer of the material i.e. ceramic material is spread along with a selective composition of the binder. The binders are selectively applied using the inkjet printing depending on the slices from the CAD file. The layer by layer deposition occurs unless the final layer is deposited. In the end, a drying procedure is carried out to remove the binders. A com-

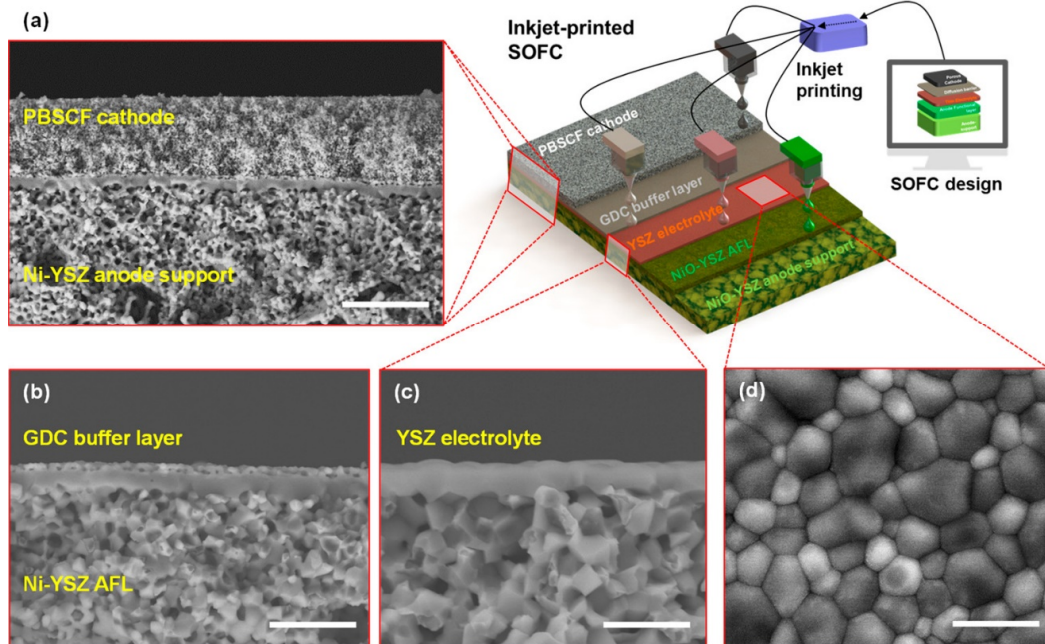


Fig. 23. SEM images of the complete cell fabricated by inkjet printing. (a) shows the complete cross-section image of the cell (scale: 10 μm) (b) shows the GDC buffer layer 0.5 μm thick (scale: 5 μm) (c) shows the cross-sectional and (d) shows the surface image of the 0.8 μm thick YSZ electrolyte(scale: 2.5 μm). Reproduced from ref. [134]

plete SOFC cell with NiO-YSZ anode, YSZ electrolyte, and LSM cathode was prepared to utilize the binder jetting technique. This additive manufacturing method did not change the material properties as it was proved from the EDS analysis that showed minimal change in composition⁹⁷⁾. The fabricated cell also showed a 98% reduction in resistance at close to an operating temperature of 750°C as compared to the lower temperature of 600°C. However, this process showed many limitations such as the electrolyte showed very low densification which led to an increase in resistance values and the OCV was also half to theoretical in this work which was attributed to gas leakage.

The most important contribution to the development of the complete single SOFC by 3D printing process is of Han et al.¹³⁴⁾. They developed complete SOFC using the inkjet printing process. The SEM images of the complete cell fabricated are shown in Fig. 23. The cells prepared showed a fine distribution of pores and grains in the anode support layer and the cathode layer. Moreover, a very dense YSZ and GDC buffer layers were also achieved. All the inks used for the inkjet printing showed good stability

over one month. The cells fabricated showed high performance of 740 mW/cm² at 650°C as shown in Fig. 24. The fabricated cells showed stable performances over 100 hours too.

It can be seen that efforts have been made in the fabrication of a complete SOFC via 3D printing processes such as inkjet printing and binder jetting. It was distinguishable that the inkjet-printed cells displayed a higher performance than the binder jetted cells. Moreover, it was also shown that the cells in which all the non-supporting layers were produced by inkjet printing displayed a performance identical to the commercially used screen printing process. Moreover, the work on the fabrication of a complete SOFC via a novel technique of binder jetting is still in its initial stages and needs further work to explore the potential of it. Considering the work of Han et al.¹³⁴⁾, the potential of 3D printing processes in the fabrication of complete SOFCs has been demonstrated. The fabrication of the complete SOFCs using the inkjet printing process will not only result in the fabrication of the SOFCs with reduced cost (which is one the main problems towards the SOFC commercialization) but also will result in improved SOFC with improved performances, reproducibility, and stable operations.

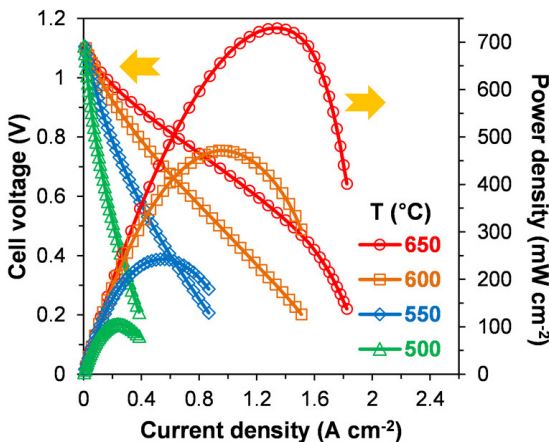


Fig. 24. Electrochemical performance of the cell produced in the ref. [134]. Reproduced from ref. [134]

6. Summary and outlook

3D printing provides immense advantages as it is an automated, simple, and accurate process that provides high geometrical freedom and good reproducibility which gives it preference over other techniques such as screen printing, tape casting, dip coating, chemical vapor deposition, and physical vapor deposition. 3-D printing processes have been successfully utilized in the production of various parts of the SOFC such as the electrolyte, anode, and cathode.

The feasibility of the 3D printing processes for the

fabrication of the electrolyte is proved by the fact that in the reported works dense and thin electrolytes have been manufactured. In the reported works for electrolyte manufacturing of the SOFCs, the inkjet printing process has been mostly utilized. However, some of the works also report the use of SLA and AJP for electrolyte fabrication purposes. These SOFCs having a 3D printed electrolyte showed high performance and good reproducibility as well. The extensive preference of the inkjet printing technique over the others to produce the electrolyte can be attributed to its low cost, and simplicity in use when compared with other techniques such as SLA and SLS. The manufacturing of the electrolyte supports by the 3D printing processes can be a huge step towards the SOFC commercialization as it significantly decreases the number of steps required for the SOFC stack formation.

Similarly, in the case of the cathode fabrication of the SOFC, the inkjet printing process has been widely utilized. Most of the work on the fabrication of the SOFC components has been on the cathode side. The SOFCs with the cathode manufactured by the inkjet printing process performed better than the cells with sputtered and paste painted cathode. It also had a similar performance to the screen-printed cathodes. Considering the advantages that the 3D printing process such as inkjet printing provides over the manual technique of screen printing, it should be preferred. AJP has also been reported for cathode fabrication. It is specifically advantageous while using the composite cathodes such as the conventional LSCF-GDC cathode, as its dual atomizer configuration eliminates the need for a time-consuming ball milling process. However, in the case of the anode fabrication of the SOFC, the reported works have been few and far between. There is a need for massive attention to the R&D of the anode supports of the SOFCs. The re-

sulting anode supports from the 3D printing process have the potential to show much improved SOFCs. The fabrication of the complete SOFC with the 3D printing process and commercialization of the process could be the missing step in the extensive commercialization of the SOFCs as it has the potential to fabricate the low-cost high performance IT SOFCs.

Without a doubt, the inkjet printing process has been the most established if the fabrication of the SOFC components is taken into account. The inks for the cathode and electrolyte have already been optimized. The parameters for the fabrication of various components have also been defined. The speed of the inkjet printing and other 3D printing processes have concerns regarding them when mass-production is considered.

The research on 3D printing of the SOFCs is still in its early stages and further efforts are required to help develop better performance SOFCs. Exploration and improvements in the 3D printing processes are required to achieve the cells with high specific power per unit mass. Moreover, the potential 3D printing processes other than inkjet printing such as SLA, SLM, and FDM, etc. should also be explored.

7. Acknowledgment

This work was supported by the Technology Development Program to Solve Climate Changes under a National Research Foundation (NRF) grant funded by the Korean government (Ministry of Science and ICT) (NRF-2020M1A2A2080867 and NRF-2017M1A2A2044926).

References

1. A. Kirubakaran, S. Jain, and R. K. Nema, "A review on fuel cell technologies and power electronic interface", *Renew. Sustain. Energy Rev.*, Vol. 13, No. 9, 2009, pp. 2430–2440.

- doi: <https://doi.org/10.1016/j.rser.2009.04.004>.
2. N. Mahato, A. Banerjee, A. Gupta, S. Omar, and K. Balani, "Progress in material selection for solid oxide fuel cell technology: a review", *Prog. Mater. Sci.*, Vol. 72, 2015, pp. 141–337, doi: <https://doi.org/10.1016/j.pmatsci.2015.01.001>.
 3. V. S. Bagotsky, "Solid-oxide fuel cells", *Fuel Cells*, 2008, pp. 135–160, doi: <https://doi.org/10.1002/9780470432204.ch8>.
 4. N. M. Sammes, Y. Du, and R. Bove, "Design and fabrication of a 100 W anode supported micro-tubular SOFC stack", *J. Power Sources*, Vol. 145, No. 2, 2005, pp. 428–434, doi: <https://doi.org/10.1016/j.jpowsour.2005.01.079>.
 5. A. Chroneos, B. Yildiz, A. Tarancón, D. Parfitt, and J. A. Kilner, "Oxygen diffusion in solid oxide fuel cell cathode and electrolyte materials: mechanistic insights from atomistic simulations", *Energy Environ. Sci.*, Vol. 4, No. 8, 2011, pp. 2774–2789, doi: <https://doi.org/10.1039/c0ee00717j>.
 6. S. P. S. Badwal and K. Foger, "Solid oxide electrolyte fuel cell review", *Ceram. Int.*, Vol. 22, No. 3, 1996, pp. 257–265, doi: [https://doi.org/10.1016/0272-8842\(95\)00101-8](https://doi.org/10.1016/0272-8842(95)00101-8).
 7. R. M. Ormerod, "Solid oxide fuel cells", *Chem. Soc. Rev.*, Vol. 32, No. 1, 2003, pp. 17–28, doi: <https://doi.org/10.1039/b105764m>.
 8. N. Q. Minh, "Ceramic fuel cells", Vol. 76, No. 3, 1993, pp. 563–588, doi: <https://doi.org/10.1111/j.1151-2916.1993.tb03645.x>.
 9. N. Q. Minh, "Solid oxide fuel cell technology—features and applications", *Solid State Ionics*, Vol. 174, No. 1–4, 2004, pp. 271–277, doi: <https://doi.org/10.1016/j.ssi.2004.07.042>.
 10. C. Hatchwell, N. M. Sammes, and I. W. M. Brown, "Fabrication and properties of $Ce_{0.8}Gd_{0.2}O_{1.9}$ electrolyte-based tubular solid oxide fuel cells", *Solid State Ionics*, Vol. 126, No. 3–4, 1999, pp. 201–208, doi: [https://doi.org/10.1016/S0167-2738\(99\)00232-5](https://doi.org/10.1016/S0167-2738(99)00232-5).
 11. F. Tietz, H. P. Buchkremer, and D. Stöver, "Components manufacturing for solid oxide fuel cells", *Solid State Ionics*, Vol. 152–153, 2002, pp. 373–381, doi: [https://doi.org/10.1016/S0167-2738\(02\)00344-2](https://doi.org/10.1016/S0167-2738(02)00344-2).
 12. S. C. Singhal, "Solid oxide fuel cells for stationary, mobile, and military applications", *Solid State Ionics*, Vol. 152–153, 2002, pp. 405–410, doi: [https://doi.org/10.1016/S0167-2738\(02\)00349-1](https://doi.org/10.1016/S0167-2738(02)00349-1).
 13. Y. Du, N. M. Sammes, G. A. Tompsett, D. Zhang, J. Swan, and M. Bowden, "Extruded Tubular Strontium- and Magnesium-Doped Lanthanum Gallate, Gadolinium-Doped Ceria, and Ytria-Stabilized Zirconia Electrolytes: Mechanical and Thermal Properties", *J. Electrochem. Soc.*, Vol. 150, No. 1, 2003, pp. A74, doi: <https://doi.org/10.1149/1.1525268>.
 14. L. S. Mahmud, A. Muchtar, and M. R. Somalu, "Challenges in fabricating planar solid oxide fuel cells: A review", *Renew. Sustain. Energy Rev.*, Vol. 72, 2017, pp. 105–116, doi: <https://doi.org/10.1016/j.rser.2017.01.019>.
 15. T. L. Cable and S. W. Sofie, "A symmetrical, planar SOFC design for NASA's high specific power density requirements", *J. Power Sources*, Vol. 174, No. 1, 2007, pp. 221–227, doi: <https://doi.org/10.1016/j.jpowsour.2007.08.110>.
 16. N. Sugita, M. Watanabe, Y. Sano, M. Terashima, and M. Mitsuishi, "Cutting tool for bone machining to carry out roughing and finishing in a single pass", *Proc. 6th Int. Conf. Lead. Edge Manuf. 21st Century, LEM 2011*, Vol. 297, 2011, pp. 103–112, doi: https://doi.org/10.1299/jsmelem.2011.6._3285-1_.
 17. B. K. Park, J. W. Lee, S. B. Lee, T. H. Lim, S. J. Park, R. H. Song, W. B. Im, and D. R. Shin, "La-doped $SrTiO_3$ interconnect materials for anode-supported flat-tubular solid oxide fuel cells", *Int. J. Hydrogen Energy*, Vol. 37, No. 5, 2012, pp. 4319–4327, doi: <https://doi.org/10.1016/j.ijhydene.2011.10.125>.
 18. F. Snijkers, A. de Wilde, S. Mullens, and J. Luyten, "Aqueous tape casting of yttria stabilised zirconia using natural product binder", *J. Eur. Ceram. Soc.*, Vol. 24, No. 6, 2004, pp. 1107–1110, doi: [https://doi.org/10.1016/S0955-2219\(03\)00388-1](https://doi.org/10.1016/S0955-2219(03)00388-1).
 19. D. Montinaro, V. M. Sglavo, M. Bertoldi, T. Zandonella, A. Aricò, M. Lo Faro, and V. Antonucci, "Tape casting fabrication and co-sintering of solid oxide "half cells" with a cathode-electrolyte porous interface", *Solid State Ionics*, Vol. 177, No. 19–25, 2006, pp. 2093–2097, doi: <https://doi.org/10.1016/j.ssi.2006.01.016>.
 20. C. Fu, S. H. Chan, Q. Liu, X. Ge, and G. Pasciak, "Fabrication and evaluation of Ni-GDC composite anode prepared by aqueous-based tape casting method for low-temperature solid oxide fuel cell", *Int. J. Hydrogen Energy*, Vol. 35, No. 1, 2010, pp. 301–307, doi: <https://doi.org/10.1016/j.ijhydene.2009.09.101>.
 21. W. S. Jang, S. H. Hyun, and S. G. Kim, "Preparation of YSZ/YDC and YSZ/GDC composite electrolytes by the tape casting and sol-gel dip-drawing coating method for low-temperature SOFC", *J. Mater. Sci.*, Vol. 37, No. 12, 2002, pp. 2535–2541, doi: <https://doi.org/10.1023/A:1015451910081>.
 22. A. Sanson, P. Pinasco, and E. Roncari, "Influence of pore formers on slurry composition and microstructure of tape cast supporting anodes for SOFCs", *J. Eur. Ceram. Soc.*, Vol. 28, No. 6, 2008, pp. 1221–1226, doi: <https://doi.org/10.1016/j.jeurceramsoc.2007.10.001>.
 23. H. Moon, S. D. Kim, E. W. Park, S. H. Hyun, and H. S. Kim, "Characteristics of SOFC single cells with anode active layer via tape casting and co-firing", *Int. J. Hydrogen Energy*, Vol. 33, No. 11, 2008, pp. 2826–2833, doi: <https://doi.org/10.1016/j.ijhydene.2008.03.024>.
 24. Z. Wang, J. Qian, J. Cao, S. Wang, and T. Wen, "A study of multilayer tape casting method for anode-supported planar type solid oxide fuel cells (SOFCs)", *J. Alloys Compd.*, Vol. 437, No. 1–2, 2007, pp. 264–268, doi:

- <https://doi.org/10.1016/j.jallcom.2006.07.110>.
25. J. H. Song, S. I. Park, J. H. Lee, and H. S. Kim, "Fabrication characteristics of an anode-supported thin-film electrolyte fabricated by the tape casting method for IT-SOFC", *J. Mater. Process. Technol.*, Vol. 198, No. 1-3, 2008, pp. 414-418, doi: <https://doi.org/10.1016/j.jmatprotec.2007.07.030>.
 26. D. Simwonis, H. Thülen, F. J. Dias, A. Naoumidis, and D. Stöver, "Properties of Ni/YSZ porous cermets for SOFC anode substrates prepared by tape casting and coat-mix[®] process", *J. Mater. Process. Technol.*, Vol. 92-93, 1999, pp. 107-111, doi: [https://doi.org/10.1016/S0924-0136\(99\)00214-9](https://doi.org/10.1016/S0924-0136(99)00214-9).
 27. H. Moon, S. D. Kim, S. H. Hyun, and H. S. Kim, "Development of IT-SOFC unit cells with anode-supported thin electrolytes via tape casting and co-firing", *Int. J. Hydrogen Energy*, Vol. 33, No. 6, 2008, pp. 1758-1768, doi: <https://doi.org/10.1016/j.ijhydene.2007.12.062>.
 28. D. Rotureau, J. P. Viricelle, C. Pijolat, N. Caillol, and M. Pijolat, "Development of a planar SOFC device using screen-printing technology", *J. Eur. Ceram. Soc.*, Vol. 25, No. 12, 2005, pp. 2633-2636, doi: <https://doi.org/10.1016/j.jeurceramsoc.2005.03.115>.
 29. C. Xia, F. Chen, and M. Liu, "Reduced-temperature solid oxide fuel cells fabricated by screen printing", *Electrochem. Solid-State Lett.*, Vol. 4, No. 5, 2001, pp. A52, doi: <https://doi.org/10.1149/1.1361158>.
 30. X. Ge, X. Huang, Y. Zhang, Z. Lu, J. Xu, K. Chen, D. Dong, Z. Liu, J. Miao, and W. Su, "Screen-printed thin YSZ films used as electrolytes for solid oxide fuel cells", *J. Power Sources*, Vol. 159, No. 2, 2006, pp. 1048-1050, doi: <https://doi.org/10.1016/j.jpowsour.2005.12.013>.
 31. Y. Zhang, J. Liu, X. Huang, Z. Lu, and W. Su, "Low temperature solid oxide fuel cell with Ba_{0.5}Sr_{0.5}Co_{0.9}Fe_{0.2}O₃ cathode prepared by screen printing", *Solid State Ionics*, Vol. 179, 2008, pp. 250-255, doi: <https://doi.org/10.1016/j.ssi.2008.02.008>.
 32. P. Ried, C. Lorenz, A. Brönstrup, T. Graule, N. H. Menzler, W. Sitte, and P. Holtappels, "Processing of YSZ screen printing pastes and the characterization of the electrolyte layers for anode supported SOFC", *J. Eur. Ceram. Soc.*, Vol. 28, No. 9, 2008, pp. 1801-1808, doi: <https://doi.org/10.1016/j.jeurceramsoc.2007.11.018>.
 33. C. Brahim, A. Ringuedé, E. Gourba, M. Cassir, A. Billard, and P. Briois, "Electrical properties of thin bilayered YSZ/GDC SOFC electrolyte elaborated by sputtering", *J. Power Sources*, Vol. 156, No. 1, 2006, pp. 45-49, doi: <https://doi.org/10.1016/j.jpowsour.2005.08.017>.
 34. G. J. La O, J. Hertz, H. Tuller, and Y. Shao-Horn, "Microstructural features of RF-sputtered SOFC anode and electrolyte materials", *J. Electroceramics*, Vol. 13, No. 1-3, 2004, pp. 691-695, doi: <https://doi.org/10.1007/s10832-004-5177-9>.
 35. K. Hayashi, O. Yamamoto, Y. Nishigaki, and H. Minoura, "Sputtered La_{0.5}Sr_{0.5}MnO₃-yttria stabilized zirconia composite film electrodes for SOFC", *Solid State Ionics*, Vol. 98, No. 1-2, 1997, pp. 49-55, doi: [https://doi.org/10.1016/S0167-2738\(97\)00098-2](https://doi.org/10.1016/S0167-2738(97)00098-2).
 36. C. L. Chu, J. Y. Wang, and S. Lee, "Effects of La_{0.67}Sr_{0.33}MnO₃ protective coating on SOFC interconnect by plasma-sputtering", *Int. J. Hydrogen Energy*, Vol. 33, No. 10, 2008, pp. 2536-2546, doi: <https://doi.org/10.1016/j.ijhydene.2008.02.061>.
 37. N. Orlovskaya, A. Coratolo, C. Johnson, and R. Gemmen, "Structural characterization of lanthanum chromite perovskite coating deposited by magnetron sputtering on an iron-based chromium-containing alloy as a promising interconnect material for SOFCs", *J. Am. Ceram. Soc.*, Vol. 87, 2005, pp. 1981-1987, doi: <https://doi.org/10.1111/j.1151-2916.2004.tb06350.x>.
 38. D. Perednis and L. J. Gauckler, "Solid oxide fuel cells with electrolytes prepared via spray pyrolysis", *Solid State Ionics*, Vol. 166, No. 3-4, 2004, pp. 229-239, doi: <https://doi.org/10.1016/j.ssi.2003.11.011>.
 39. T. Setoguchi, M. Sawano, K. Eguchi, and H. Arai, "Application of the stabilized zirconia thin film prepared by spray pyrolysis method to SOFC", *Solid State Ionics*, Vol. 40-41, 1990, pp. 502-505, doi: [https://doi.org/10.1016/0167-2738\(90\)90390-D](https://doi.org/10.1016/0167-2738(90)90390-D).
 40. D. Beckel, U. P. Muecke, T. Gyger, G. Florey, A. Infortuna, and L. J. Gauckler, "Electrochemical performance of LSCF based thin film cathodes prepared by spray pyrolysis", *Solid State Ionics*, Vol. 178, No. 5-6, 2007, pp. 407-415, doi: <https://doi.org/10.1016/j.ssi.2007.01.019>.
 41. A. O. Stoermer, J. L. M. Rupp, and L. J. Gauckler, "Spray pyrolysis of electrolyte interlayers for vacuum plasma-sprayed SOFC", *Solid State Ionics*, Vol. 177, No. 19-25 SPEC. ISS., pp. 2075-2079, 2006, doi: <https://doi.org/10.1016/j.ssi.2006.06.033>.
 42. S. Suda, M. Itagaki, E. Node, S. Takahashi, M. Kawano, H. Yoshida, and T. Inagaki, "Preparation of SOFC anode composites by spray pyrolysis", *J. Eur. Ceram. Soc.*, Vol. 26, No. 4-5, 2006, pp. 593-597, doi: <https://doi.org/10.1016/j.jeurceramsoc.2005.07.038>.
 43. P. Gannon, M. Deibert, P. White, R. Smith, H. Chen, W. Priyantha, J. Lucas, and V. Gorokhovskiy, "Advanced PVD protective coatings for SOFC interconnects", *Int. J. Hydrogen Energy*, Vol. 33, No. 14, 2008, pp. 3991-4000, doi: <https://doi.org/10.1016/j.ijhydene.2007.12.009>.
 44. V. I. Gorokhovskiy, P. E. Gannon, M. C. Deibert, R. J. Smith, A. Kayani, M. Kocpczyk, D. VanVorous, Zhenguo Yang, J. W. Stevenson, S. Visco, C. Jacobson, H. Kurokawa, and S. W. Sofie, "Deposition and evaluation of protective pvd coatings on ferritic stainless steel SOFC interconnects", *J. Electrochem. Soc.*, Vol. 153, No. 10, 2006, pp. A1886, doi:

- <https://doi.org/10.1149/1.2266244>.
45. H. Y. Jung, K. S. Hong, H. Kim, J. K. Park, J. W. Son, J. Kim, H. W. Lee, and J. H. Lee, "Characterization of thin-film YSZ deposited via EB-PVD technique in anode-supported SOFCs", *J. Electrochem. Soc.*, Vol. 153, No. 6, 2006, pp. A961, doi: <https://doi.org/10.1149/1.2186209>.
 46. Y. Liu, S. Zha, and M. Liu, "Novel nanostructured electrodes for solid oxide fuel cells fabricated by combustion chemical vapor deposition (CVD)", *Adv. Mater.*, Vol. 16, No. 3, 2004, pp. 256-260, doi: <https://doi.org/10.1002/adma.200305767>.
 47. Y. Liu, W. Rauch, S. Zha, and M. Liu, "Fabrication of $\text{Sm}_{0.5}\text{Sr}_{0.5}\text{CoO}_{3-\delta}$ - $\text{Sm}_{0.1}\text{Ce}_{0.9}\text{O}_{2-\delta}$ cathodes for solid oxide fuel cells using combustion CVD", *Solid State Ionics*, Vol. 166, No. 3-4, 2004, pp. 261-268, doi: <https://doi.org/10.1016/j.ssi.2003.12.001>.
 48. T. Takeyama, N. Takahashi, T. Nakamura, and S. Itoh, " δ - Bi_2O_3 thin films deposited on dense YSZ substrates by CVD method under atmospheric pressure for intermediate temperature SOFC applications", *Surf. Coatings Technol.*, Vol. 200, No. 16-17, 2006, pp. 4797-4801, doi: <https://doi.org/10.1016/j.surfcoat.2005.04.047>.
 49. G. Meng, H. Song, C. Xia, X. Liu, and D. Peng, "Novel CVD techniques for Micro- and IT-SOFC fabrication", *Fuel Cells*, Vol. 4, No. 1-2, 2004, pp. 48-55, doi: <https://doi.org/10.1002/face.200400006>.
 50. G. Y. Meng, H. Z. Song, H. B. Wang, C. R. Xia, and D. K. Peng, "Progress in ion-transport inorganic membranes by novel chemical vapor deposition (CVD) techniques", *Thin Solid Films*, Vol. 409, No. 1, 2002, pp. 105-111, doi: [https://doi.org/10.1016/S0040-6090\(02\)00111-6](https://doi.org/10.1016/S0040-6090(02)00111-6).
 51. L. Jia, Z. Lü, X. Huang, Z. Liu, K. Chen, X. Sha, G. Li, and W. Su, "Preparation of YSZ film by EPD and its application in SOFCs", *J. Alloys Compd.*, Vol. 424, No. 1-2, 2006, pp. 299-303, doi: <https://doi.org/10.1016/j.jallcom.2005.12.065>.
 52. M. Matsuda, T. Hosomi, K. Murata, T. Fukui, and M. Miyake, "Direct EPD of YSZ electrolyte film onto porous NiO-YSZ composite substrate for reduced-temperature operating anode-supported SOFC", *Electrochem. Solid-State Lett.*, Vol. 8, No. 1, 2005, pp. A8, doi: <https://doi.org/10.1149/1.1828342>.
 53. K. Yamaji, H. Kishimoto, Y. Xiong, T. Horita, N. Sakai, and H. Yokokawa, "Performance of anode-supported SOFCs fabricated with EPD techniques", *Solid State Ionics*, Vol. 175, No. 1-4, 2004, pp. 165-169, doi: <https://doi.org/10.1016/j.ssi.2004.09.032>.
 54. C. Li, H. Shi, R. Ran, C. Su, and Z. Shao, "Thermal inkjet printing of thin-film electrolytes and buffering layers for solid oxide fuel cells with improved performance", *Int. J. Hydrogen Energy*, Vol. 38, No. 22, 2013, pp. 9310-9319, doi: <https://doi.org/10.1016/j.ijhydene.2013.05.025>.
 55. M. Sureshini A., F. Meisenkothen, P. Gardner, and T. L. Reitz, "Aerosol Jet[®] Printing of functionally graded SOFC anode interlayer and microstructural investigation by low voltage scanning electron microscopy", *J. Power Sources*, 2013, Vol. 224, pp. 295-303, doi: <https://doi.org/10.1016/j.jpowsour.2012.09.094>.
 56. M. R. Weimar, L. A. Chick, D. W. Gotthold, and G. A. Whyatt, "Cost study for manufacturing of solid oxide fuel cell power systems", 2013, doi: <https://doi.org/10.2172/1126362>.
 57. A. Casanova, "A consortium approach to commercialized Westinghouse solid oxide fuel cell technology", *J. Power Sources*, Vol. 71, No. 1-2, 1998, pp. 65-70, doi: [https://doi.org/10.1016/S0378-7753\(97\)02757-2](https://doi.org/10.1016/S0378-7753(97)02757-2).
 58. K. Horiuchi, "Current status of national SOFC projects in Japan", *ECS Transactions*, Vol. 57, No. 1, pp. 3-10, 2013, <https://iopscience.iop.org/article/10.1149/05701.0003ecst>.
 59. M. Kadowaki, "Current status of national SOFC projects in Japan", *ECS Transactions*, Vol. 68, No. 1, pp. 15-22, 2015, <https://iopscience.iop.org/article/10.1149/06801.0015ecst>.
 60. B. Zhu, "Next generation fuel cell R&D", *Int. J. Energy Res.*, Vol. 30, No. 11, 2006, pp. 895-903, doi: <https://doi.org/10.1002/er.1195>.
 61. C. Schubert, M. C. Van Langeveld, and L. A. Donoso, "Innovations in 3D printing: a 3D overview from optics to organs", *Br. J. Ophthalmol.*, Vol. 98, No. 2, 2014, pp. 159-161, doi: <https://doi.org/10.1136/bjophthalmol-2013-304446>.
 62. M. Vaezi and C. K. Chua, "Effects of layer thickness and binder saturation level parameters on 3D printing process", *Int. J. Adv. Manuf. Technol.*, Vol. 53, No. 1-4, 2011, pp. 275-284, doi: <https://doi.org/10.1007/s00170-010-2821-1>.
 63. M. N. Jahangir, M. A. H. Mamun, and M. P. Sealy, "A review of additive manufacturing of magnesium alloys", *AIP Conf. Proc.*, Vol. 1980, No. 1, 2018, doi: <https://doi.org/10.1063/1.5044305>.
 64. B. Berman, "3-D printing: the new industrial revolution", *Bus. Horiz.*, Vol. 55, No. 2, 2012, pp. 155-162, doi: <https://doi.org/10.1016/j.bushor.2011.11.003>.
 65. V. Petrovic, J. V. H. Gonzalez, O. J. Ferrando, J. D. Gordillo, J. R. B. Puchades, and L. P. Griñan, "Additive layered manufacturing: sectors of industrial application shown through case studies", Vol. 49, No.4, 2011, pp. 1061-1079, doi: <https://doi.org/10.1080/00207540903479786>.
 66. P. Calvert, "Inkjet printing for materials and devices", *Chem. Mater.*, Vol. 13, No. 10, 2001, pp. 3299-3305, doi: <https://doi.org/10.1021/cm0101632>.
 67. R. I. Tomov, M. Krauz, J. Jewulski, S. C. Hopkins, J. R. Kluczowski, D. M. Glowacka, and B. A. Glowacki, "Direct ceramic inkjet printing of yttria-stabilized zirconia electrolyte layers for anode-supported solid oxide fuel cells", *J. Power Sources*, Vol. 195, No. 21, 2010, pp. 7160-7167, doi:

- <https://doi.org/10.1016/j.jpowsour.2010.05.044>.
68. M. A. Sukeshini, R. Cummins, T. L. Reitz, and R. M. Miller, "Inkjet printing: a versatile method for multilayer solid oxide fuel cells fabrication", *J. Am. Ceram. Soc.*, Vol. 92, No. 12, 2009, pp. 2913–2919, doi: <https://doi.org/10.1111/j.1551-2916.2009.03349.x>.
 69. E. A. Roth, T. Xu, M. Das, C. Gregory, J. J. Hickman, and T. Boland, "Inkjet printing for high-throughput cell patterning", *Biomaterials*, Vol. 25, No. 17, 2004, pp. 3707–3715, doi: <https://doi.org/10.1016/j.biomaterials.2003.10.052>.
 70. V. Esposito, C. Gadea, J. Hjelm, D. Marani, Q. Hu, K. Agersted, S. Ramousse, and S. H. Jensen, "Fabrication of thin yttria-stabilized-zirconia dense electrolyte layers by inkjet printing for high performing solid oxide fuel cells", *J. Power Sources*, Vol. 273, 2015, pp. 89–95, doi: <https://doi.org/10.1016/j.jpowsour.2014.09.085>.
 71. G. D. Han, K. C. Neoh, K. Bae, H. J. Choi, S. W. Park, J. W. Son, and J. H. Shim, "Fabrication of lanthanum strontium cobalt ferrite (LSCF) cathodes for high performance solid oxide fuel cells using a low price commercial inkjet printer", *J. Power Sources*, Vol. 306, 2016, pp. 503–509, doi: <https://doi.org/10.1016/j.jpowsour.2015.12.067>.
 72. G. Cummins and M. P. Y. Desmulliez, "Inkjet printing of conductive materials: a review", *Circuit World*, Vol. 38, No. 4, 2012, pp. 193–213, doi: <https://doi.org/10.1108/03056121211280413>.
 73. J. E. Fromm, "Numerical calculation of the fluid dynamics of drop-on-demand jets", *IBM J. Res. Dev.*, Vol. 28, 1984, pp. 322–333.
 74. N. Reis and B. Derby, "Ink jet deposition of ceramic suspensions: modeling and experiments of droplet formation", *MRS Proceedings*, Vol. 624, 2000, pp. 65, doi: <https://doi.org/10.1557/PROC-624-65>.
 75. D. Zhao, T. Liu, M. Zhang, R. Liang, and B. Wang, "Fabrication and characterization of aerosol-jet printed strain sensors for multifunctional composite structures", *Smart Mater. Struct.*, Vol. 21, No. 11, 2012, doi: <https://doi.org/10.1088/0964-1726/21/11/115008>.
 76. A. Mahajan, C. D. Frisbie, and L. F. Francis, "Optimization of aerosol jet printing for high-resolution, high-aspect ratio silver lines", *ACS Appl. Mater. Interfaces*, Vol. 5, No. 11, 2013, pp. 4856–4864, doi: <https://doi.org/10.1021/am400606y>.
 77. D. W. Hutmacher, T. Schantz, I. Zein, K. W. Ng, S. H. Teoh, and K. C. Tan, "Mechanical properties and cell cultural response of polycaprolactone scaffolds designed and fabricated via fused deposition modeling", *J. Biomed. Mater. Res.*, Vol. 55, No. 2, 2001, pp. 203–216, doi: [https://doi.org/10.1002/1097-4636\(200105\)55:2<203::AID-JBM1007>3.0.CO;2-7](https://doi.org/10.1002/1097-4636(200105)55:2<203::AID-JBM1007>3.0.CO;2-7).
 78. O. A. Mohamed, S. H. Masood, and J. L. Bhowmik, "Optimization of fused deposition modeling process parameters: a review of current research and future prospects", *Adv. Manuf.*, Vol. 3, No. 1, 2015, pp. 42–53, doi: <https://doi.org/10.1007/s40436-014-0097-7>.
 79. M. L. Shofner, K. Lozano, F. J. Rodríguez-Macias, and E. V. Barrera, "Nanofiber-reinforced polymers prepared by fused deposition modeling", *J. Appl. Polym. Sci.*, Vol. 89, No. 11, 2003, pp. 3081–3090, doi: <https://doi.org/10.1002/app.12496>.
 80. I. Zein, D. W. Hutmacher, K. C. Tan, and S. H. Teoh, "Fused deposition modeling of novel scaffold architectures for tissue engineering applications", *Biomaterials*, Vol. 23, No. 4, 2002, pp. 1169–1185, doi: [https://doi.org/10.1016/S0142-9612\(01\)00232-0](https://doi.org/10.1016/S0142-9612(01)00232-0).
 81. X. Yan and P. Gu, "A review of rapid prototyping technologies and systems", *Computer-Aided Design*, Vol. 28, No. 4, 1996, pp. 307–318, doi: [https://doi.org/10.1016/0010-4485\(95\)00035-6](https://doi.org/10.1016/0010-4485(95)00035-6).
 82. B. Dhariwala, E. Hunt, and T. Boland, "Rapid prototyping of tissue-engineering constructs, using photopolymerizable hydrogels and stereolithography", *Tissue Engineering*, Vol. 10, No. 9–10, 2004, pp. 1316–1322, doi: <https://doi.org/10.1089/ten.2004.10.1316>.
 83. H. Wu, W. Liu, R. He, Z. Wu, Q. Jiang, X. Song, Y. Chen, L. Cheng, and S. Wu, "Fabrication of dense zirconia-toughened alumina ceramics through a stereolithography-based additive manufacturing", *Ceram. Int.*, Vol. 43, No. 1, 2017, pp. 968–972, doi: <https://doi.org/10.1016/j.ceramint.2016.10.027>.
 84. P. Jacobs, "Stereolithography 1993: epoxy resins, improved accuracy, and investment casting", *Proc. SPIE 2102, Coupling Technology to National Need, 1994*, doi: <https://doi.org/10.1117/12.170612>.
 85. F. P. W. Melchels, J. Feijen, and D. W. Grijpma, "A review on stereolithography and its applications in biomedical engineering", *Biomaterials*, Vol. 31, No. 24, 2010, pp. 6121–6130, doi: <https://doi.org/10.1016/j.biomaterials.2010.04.050>.
 86. J. M. Williams, A. Adewunmi, R. M. Schek, C. L. Flanagan, P. H. Krebsbach, S. E. Feinberg, S. J. Hollister, and S. Das, "Bone tissue engineering using polycaprolactone scaffolds fabricated via selective laser sintering", *Biomaterials*, Vol. 26, No. 23, 2005, pp. 4817–4827, doi: <https://doi.org/10.1016/j.biomaterials.2004.11.057>.
 87. K. A. Sidarto, A. Kania, and N. Sumarti, "Finding multiple solutions of multimodal optimization using spiral optimization algorithm with clustering", *Mendel*, Vol. 23, No. 1, 2017, pp. 95–102, doi: <https://doi.org/10.13164/mendel.2017.1.095>.
 88. S. F. S. Shirazi, S. Gharehkhani, M. Mehrali, H. Yarmand, H. S. C. Metselaar, N. A. Kadri, and N. A. A. Osman, "A review on powder-based additive manufacturing for tissue engineering: Selective laser sintering and inkjet 3D print –

- ing”, *Sci. Technol. Adv. Mater.*, Vol. 16, No. 3, 2015, doi: <https://doi.org/10.1088/1468-6996/16/3/033502>.
89. M. Vaezi, H. Seitz, and S. Yang, “A review on 3D micro-additive manufacturing technologies”, *Int. J. Adv. Manuf. Technol.*, Vol. 67, No. 5-8, 2013, pp. 1721-1754, doi: <https://doi.org/10.1007/s00170-012-4605-2>.
 90. S. Eshraghi and S. Das, “Mechanical and microstructural properties of polycaprolactone scaffolds with one-dimensional, two-dimensional, and three-dimensional orthogonally oriented porous architectures produced by selective laser sintering”, *Acta Biomater.*, Vol. 6, No. 7, 2010, pp. 2467-2476, doi: <https://doi.org/10.1016/j.actbio.2010.02.002>.
 91. J. C. Ruiz-Morales, A. Tarancón, J. Canales-Vázquez, J. Méndez-Ramos, L. Hernández-Afonso, P. Acosta-Mora, J. R. M. Ruedac, and R. Fernández-González, “Three dimensional printing of components and functional devices for energy and environmental applications”, *Energy Environ. Sci.*, Vol. 10, No. 4, 2017, pp. 846-859, doi: <https://doi.org/10.1039/c6ee03526d>.
 92. J. Will, A. Mitterdorfer, C. Kleinlogel, D. Perednis, and L. J. Gauckler, “Fabrication of thin electrolytes for second-generation solid oxide fuel cells”, *Solid State Ionics*, Vol. 131, No. 1-2, 2000, pp. 79-96, doi: [https://doi.org/10.1016/S0167-2738\(00\)00624-X](https://doi.org/10.1016/S0167-2738(00)00624-X).
 93. J. S. Kim, M. H. Cho, S. C. Lee, J. H. Pang, J. H. Lee, and A. Ohki, “Lead selective lipophilic acyclic diionizable polyethers”, *Talanta*, Vol. 49, No. 1, 1999, pp. 69-75, doi: [https://doi.org/10.1016/S0039-9140\(98\)00362-2](https://doi.org/10.1016/S0039-9140(98)00362-2).
 94. S. de Souza, S. J. Visco, and L. C. De Jonghe, “Thin-film solid oxide fuel cell with high performance at low-temperature”, *Solid State Ionics*, Vol. 98, No. 1-2, 1997, pp. 57-61, doi: [https://doi.org/10.1016/S0167-2738\(96\)00525-5](https://doi.org/10.1016/S0167-2738(96)00525-5).
 95. S. Kirihara, “Creation of functional ceramics structures by using stereolithographic 3D printing”, *Trans. JWRI*, Vol. 43, No. 1, 2014, pp. 5-10.
 96. E. M. Hernández-Rodríguez, P. Acosta-Mora, J. Méndez-Ramos, E. B. Chinae, P. E. Ferrera, J. Canales-Vázquez, P. Núñez, and J. C. Ruiz-Morales, “Prospective use of the 3D printing technology for the microstructural engineering of solid oxide fuel cell components”, *Bol. Soc. Esp. Ceram. Vidr.*, Vol. 53, No. 5, 2014, pp. 213-216, doi: <https://doi.org/10.3989/cyv.252014>.
 97. G. Manogharan, M. Kioko, and C. Linkous, “Binder jetting: a novel solid oxide fuel-cell fabrication process and evaluation”, *Jom*, Vol. 67, No. 3, 2015, pp. 660-667, doi: <https://doi.org/10.1007/s11837-015-1296-9>.
 98. D. Young, A. M. Sukeshini, R. Cummins, H. Xiao, M. Rottmayer, and T. Reitz, “Ink-jet printing of electrolyte and anode functional layer for solid oxide fuel cells”, *J. Power Sources*, Vol. 184, No. 1, 2008, pp. 191-196, doi: <https://doi.org/10.1016/j.jpowsour.2008.06.018>.
 99. C. Wang, S. C. Hopkins, R. I. Tomov, R. V. Kumar, and B. A. Glowacki, “Optimisation of CGO suspensions for inkjet-printed SOFC electrolytes”, *J. Eur. Ceram. Soc.*, Vol. 32, No. 10, 2012, pp. 2317-2324, doi: <https://doi.org/10.1016/j.jeurceramsoc.2012.03.001>.
 100. A. M. El-Toni, T. Yamaguchi, S. Shimizu, Y. Fujishiro, and M. Awano, “Development of a dense electrolyte thin film by the inkjet printing technique for a porous LSM substrate”, *J. Am. Ceram. Soc.*, Vol. 91, No. 1, 2008, pp. 346-349, doi: <https://doi.org/10.1111/j.1551-2916.2007.02151.x>.
 101. M. Dudek, R. I. Tomov, C. Wang, B. A. Glowacki, P. Tomczyk, R. P. Socha, and M. Mosialek, “Feasibility of direct carbon solid oxide fuels cell (DC-SOFC) fabrication by inkjet printing technology”, *Electrochim. Acta*, Vol. 105, 2013, pp. 412-418, doi: <https://doi.org/10.1016/j.electacta.2013.04.139>.
 102. N. M. Farandos, L. Kleiminger, T. Li, A. Hankin, and G. H. Kelsall, “Three-dimensional inkjet printed solid oxide electrochemical reactors. I. Ytria-stabilized zirconia electrolyte”, *Electrochim. Acta*, Vol. 213, 2016, pp. 324-331, doi: <https://doi.org/10.1016/j.electacta.2016.07.103>.
 103. C. Wang, R. I. Tomov, R. V. Kumar, and B. A. Glowacki, “Inkjet printing of gadolinium-doped ceria electrolyte on NiO-YSZ substrates for solid oxide fuel cell applications”, *J. Mater. Sci.*, Vol. 46, No. 21, 2011, pp. 6889-6896, doi: <https://doi.org/10.1007/s10853-011-5653-y>.
 104. R. I. Tomov, M. Krauz, A. Tluczek, R. Kluczowski, Venkatesan V. Krishnan, K. Balasubramanian, R. V. Kumar, and B. A. Glowacki, “Vacuum-sintered stainless steel porous supports for inkjet printing of functional SOFC coatings”, *Mater. Renew. Sustain. Energy*, Vol. 4, No. 3, 2015, pp. 4-14, doi: <https://doi.org/10.1007/s40243-015-0056-7>.
 105. A. M. Sukeshini, P. Gardner, F. Meisenkothen, T. Jenkins, R. Miller, M. Rottmayer, and T. L. Reitz, “Aerosol jet printing and microstructure of SOFC electrolyte and cathode layers”, *ECS Trans.*, Vol. 35, No. 1, 2011, pp. 2151-2160, doi: <https://doi.org/10.1149/1.3570207>.
 106. A. M. Sukeshini, R. Cummins, T. L. Reitz, and R. M. Miller, “Inkjet printing of anode supported SOFC: comparison of slurry pasted cathode and printed cathode”, *Electrochem. Solid-State Lett.*, Vol. 12, No. 12, 2009, pp. B176, doi: <https://doi.org/10.1149/1.3243468>.
 107. R. I. Tomov, R. Duncan, M. Krauz, R. V. Kumar, and B. A. Glowacki, “Inkjet printing and inkjet infiltration of functional coatings for SOFCs fabrication”, *E3S Web Conf. SEED 2016*, Vol. 10, p. 000098, 2016, doi: <https://doi.org/10.1051/e3sconf/20161000098>.
 108. J. Liu and S. Bai, “Femtosecond laser additive manufacturing of YSZ”, *Appl. Phys. A Mater. Sci. Process.*, Vol. 123, No. 4, pp. 1-8, 2017, doi: <https://doi.org/10.1007/s00339-017-0929-y>.

109. Y. Xu, N. Farandos, M. Rosa, P. Zielke, V. Esposito, P. V. Hendriksen, S. H. Jensen, T. Li, G. Kelsall, and R. Kiebach, "Continuous hydrothermal flow synthesis of Gd-doped CeO₂ (GDC) nanoparticles for inkjet printing of SOFC electrolytes", *Int. J. Appl. Ceram. Technol.*, Vol. 15, No. 2, 2018, pp. 315–327, doi: <https://doi.org/10.1111/ijac.12845>.
110. S. Masciandaro, M. Torrell, P. Leone, and A. Taracón, "Three-dimensional printed yttria-stabilized zirconia self-supported electrolytes for solid oxide fuel cell applications", *J. Eur. Ceram. Soc.*, Vol. 39, No. 1, pp. 9–16, 2019, doi: <https://doi.org/10.1016/j.jeurceramsoc.2017.11.033>.
111. A. Arabac and M. F. Öksüzömer, "Preparation and characterization of 10 mol% Gd doped CeO₂ (GDC) electrolyte for SOFC applications", *Ceram. Int.*, Vol. 38, No. 8, pp. 6509–6515, 2012, doi: <https://doi.org/10.1016/j.ceramint.2012.05.030>.
112. A. B. Stambouli and E. Traversa, "Solid oxide fuel cells (SOFCs): a review of an environmentally clean and efficient source of energy", *Renew. Sustain. Energy Rev.*, Vol. 6, No. 5, pp. 433–455, 2002, doi: [https://doi.org/10.1016/S1364-0321\(02\)00014-X](https://doi.org/10.1016/S1364-0321(02)00014-X).
113. W. B. Russel, N. Wu, and W. Man, "Generalized Hertzian model for the deformation and cracking of colloidal packings saturated with liquid", *Langmuir*, Vol. 24, No. 5, pp. 1721–1730, 2008, doi: <https://doi.org/10.1021/la702633t>.
114. A. Pesce, A. Homés, M. Núñez, A. Morata, M. Torrell, and A. Taracón, "3D printing the next generation of enhanced solid oxide fuel and electrolysis cells", *J. Mater. Chem. A*, 2020, doi: <https://doi.org/10.1039/d0ta02803g>.
115. C. C. Chao, C. M. Hsu, Y. Cui, and F. B. Prinz, "Improved solid oxide fuel cell performance with nanostructured electrolytes", *ACS Nano*, Vol. 5, No. 7, pp. 5692–5696, 2011, doi: <https://doi.org/10.1021/nn201354p>.
116. P. C. Su, C. C. Chao, J. H. Shim, R. Fasching, and F. B. Prinz, "Solid oxide fuel cell with corrugated thin film electrolyte", *Nano Lett.*, Vol. 8, No. 8, pp. 2289–2292, 2008, doi: <https://doi.org/10.1021/nl800977z>.
117. B. Xing, C. Cao, W. Zhao, M. Shen, C. Wang, and Z. Zhao, "Dense 8 mol% yttria-stabilized zirconia electrolyte by DLP stereolithography", *J. Eur. Ceram. Soc.*, Vol. 40, No. 4, pp. 1418–1423, 2020, doi: <https://doi.org/10.1016/j.jeurceramsoc.2019.09.045>.
118. B. Xing, Y. Yao, X. Meng, W. Zhao, M. Shen, S. Gao, and Z. Zhao, "Self-supported yttria-stabilized zirconia ripple-shaped electrolyte for solid oxide fuel cells application by digital light processing three-dimension printing", *Scr. Mater.*, Vol. 181, 2020, pp. 62–65, doi: <https://doi.org/10.1016/j.scriptamat.2020.02.004>.
119. L. Wei, J. Zhang, F. Yu, W. Zhang, X. Meng, N. Yang, and S. Liu, "A novel fabrication of yttria-stabilized-zirconia dense electrolyte for solid oxide fuel cells by 3D printing technique", *Int. J. Hydrogen Energy*, Vol. 44, No. 12, 2019, pp. 6182–6191, doi: <https://doi.org/10.1016/j.ijhydene.2019.01.071>.
120. Z. Feng, L. Liu, L. Li, J. Chen, Y. Liu, Y. Li, L. Hao, and Y. Wu, "3D printed Sm-doped ceria composite electrolyte membrane for low temperature solid oxide fuel cells", *Int. J. Hydrogen Energy*, Vol. 44, No. 26, 2019, pp. 13843–13851, doi: <https://doi.org/10.1016/j.ijhydene.2019.03.254>.
121. W. Z. Zhu and S. C. Deevi, "A review on the status of anode materials for solid oxide fuel cells", *Mater. Sci. Eng. A*, Vol. 362, No. 1–2, 2003, pp. 228–239, doi: [https://doi.org/10.1016/S0921-5093\(03\)00620-8](https://doi.org/10.1016/S0921-5093(03)00620-8).
122. G. Kim, S. Lee, J. Y. Shin, G. Corre, J. T. S. Irvine, J. M. Vohs, and R. J. Gorte, "The electrochemical society investigation of the structural and catalytic requirements for high-performance SOFC anodes formed by infiltration of LSCM", *Electrochem. Solid-State Lett.*, Vol. 12, No. 3, 2009, pp. B48, doi: <https://doi.org/10.1149/1.3065971>.
123. A. Atkinson, S. Barnett, R. J. Gorte, J. T. S. Irvine, A. J. McEvoy, M. Mogensen, S. C. Singhal, and J. Vohs, "Advanced anodes for high-temperature fuel cells", *Mater. Sustain. Energy*, Vol. 3, 2010, pp. 213–223, doi: <https://doi.org/10.1038/nmat1040>.
124. Z. Liu, B. Liu, D. Ding, M. Liu, F. Chen, and C. Xia, "Review fabrication and modification of solid oxide fuel cell anodes via wet impregnation/infiltration technique", *J. Power Sources*, Vol. 237, 2013, pp. 243–259, doi: <https://doi.org/10.1016/j.jpowsour.2013.03.025>.
125. R. J. Gorte and J. M. Vohs, "Nanostructured anodes for solid oxide fuel cells", *Curr. Opin. Colloid Interface Sci.*, Vol. 14, No. 4, 2009, pp. 236–244, doi: <https://doi.org/10.1016/j.cocis.2009.04.006>.
126. S. P. Jiang, "A review of wet impregnation—an alternative method for the fabrication of high performance and nano-structured electrodes of solid oxide fuel cells", *Mater. Sci. Eng. A*, Vol. 418, No. 1–2, 2006, pp. 199–210, doi: <https://doi.org/10.1016/j.msea.2005.11.052>.
127. E. D. Wachsman and K. T. Lee, "Lowering the temperature of solid oxide fuel cells", *Science*, Vol. 334, No. 6058, 2011, pp. 935–939, doi: <https://doi.org/10.1126/science.1204090>.
128. S. Guo, H. Wu, F. Puleo, and L. Liotta, "B-site metal (Pd, Pt, Ag, Cu, Zn, Ni) promoted La_{1-x}Sr_xCo_{1-y}Fe_yO_{3±δ} perovskite oxides as cathodes for IT-SOFCs", *Catalysts*, Vol. 5, No. 1, 2015, pp. 366–391, doi: <https://doi.org/10.3390/catal5010366>.
129. D. Ding, X. Li, S. Y. Lai, K. Gerdes, and M. Liu, "Enhancing SOFC cathode performance by surface modification through infiltration", *Energy Environ. Sci.*, Vol. 7, No. 2, pp. 552–575, 2014, doi: <https://doi.org/10.1039/c3ee42926a>.
130. J. P. P. Huijsmans, F. P. F. Van Berkel, and G. M. Christie, "Intermediate temperature SOFC – a promise for the 21st

- century”, *J. Power Sources*, Vol. 71, No. 1–2, 1998, pp. 107–110, doi: [https://doi.org/10.1016/S0378-7753\(97\)02789-4](https://doi.org/10.1016/S0378-7753(97)02789-4).
131. S. D. Kim, S. H. Hyun, J. Moon, J. H. Kim, and R. H. Song, “Fabrication and characterization of anode-supported electrolyte thin films for intermediate temperature solid oxide fuel cells”, *J. Power Sources*, Vol. 139, No. 1–2, 2005, pp. 67–72, doi: <https://doi.org/10.1016/j.jpowsour.2004.07.013>.
 132. B. S. Prakash, S. S. Kumar, and S. T. Aruna, “Properties and development of Ni/YSZ as an anode material in solid oxide fuel cell: a review”, *Renew. Sustain. Energy Rev.*, Vol. 36, 2014, pp. 149–179, doi: <https://doi.org/10.1016/j.rser.2014.04.043>.
 133. K. Miyamoto, H. Koga, M. Izumi, M. Mizui, and H. Nishiguchi, “Study on fabrication of anodes for SOFCs with 3D printing technology”, *ECS Trans.*, Vol. 96, No. 1, 2020, pp. 219–226, doi: <https://doi.org/10.1149/09601.0219ecst>.
 134. G. D. Han, K. Bae, E. H. Kang, H. J. Choi, and J. H. Shim, “Inkjet printing for manufacturing solid oxide fuel cells”, *ACS Energy Lett.*, Vol. 5, No. 5, 2020, pp. 1586–1592, doi: <https://doi.org/10.1021/acseenergylett.0c00721>.
 135. C. Wang, R. I. Tomov, T. B. Mitchell-Williams, R. V. Kumar, and B. A. Glowacki, “Inkjet printing infiltration of Ni-Gd:CeO₂ anodes for low temperature solid oxide fuel cells”, *J. Appl. Electrochem.*, Vol. 47, No. 11, 2017, pp. 1227–1238, doi: <https://doi.org/10.1007/s10800-017-1114-x>.
 136. T. B. Mitchell-Williams, R. I. Tomov, S. A. Saadabadi, M. Krauz, P. V. Aravind, B. A. Glowacki, and R. V. Kumar, “Infiltration of commercially available, anode supported SOFCs via inkjet printing”, *Mater. Renew. Sustain. Energy*, Vol. 6, No. 2, 2017, pp. 1–9, doi: <https://doi.org/10.1007/s40243-017-0096-2>.
 137. C. Sun, R. Hui, and J. Roller, “Cathode materials for solid oxide fuel cells: a review”, *J. Solid State Electrochem.*, Vol. 14, No. 7, pp. 1125–1144, 2010, doi: <https://doi.org/10.1007/s10008-009-0932-0>.
 138. Y. Zhang, Q. Sun, C. Xia, and M. Ni, “Geometric properties of nanostructured solid oxide fuel cell electrodes”, *J. Electrochem. Soc.*, Vol. 160, No. 3, 2013, pp. F278–F289, doi: <https://doi.org/10.1149/2.057303jes>.
 139. H. Sumi, T. Yamaguchi, K. Hamamoto, T. Suzuki, and Y. Fujishiro, “High performance of La_{0.6}Sr_{0.4}Co_{0.2}Fe_{0.8}O_{3-δ}-Ce_{0.9}Gd_{0.1}O_{1.95} nanoparticulate cathode for intermediate temperature microtubular solid oxide fuel cells”, *J. Power Sources*, Vol. 226, 2013, pp. 354–358, doi: <https://doi.org/10.1016/j.jpowsour.2012.11.015>.
 140. B. Huang, X. J. Zhu, Y. Lv, and H. Liu, “High-performance Gd_{0.2}Ce_{0.8}O₂-impregnated LaNi_{0.6}Fe_{0.4}O_{3-δ} cathodes for intermediate temperature solid oxide fuel cell”, *J. Power Sources*, Vol. 209, 2012, pp. 209–219, doi: <https://doi.org/10.1016/j.jpowsour.2012.02.103>.
 141. Q. Li, L. P. Sun, L. H. Huo, H. Zhao, and J. C. Grenier, “Electrochemical performance of La_{1.6}Sr_{0.4}NiO₄-Ag composite cathodes for intermediate-temperature solid oxide fuel cells”, *J. Power Sources*, Vol. 196, No. 4, 2011, pp. 1712–1716, doi: <https://doi.org/10.1016/j.jpowsour.2010.10.032>.
 142. E. H. Da’as, J. T. S. Irvine, E. Traversa, and S. Bouffrad, “Controllable impregnation via inkjet printing for the fabrication of solid oxide cell air electrodes”, *ECS Trans.*, Vol. 57, No. 1, 2013, pp. 1851–1857, doi: <https://doi.org/10.1149/05701.1851ecst>.
 143. R. I. Tomov, T. Mitchell-Williams, C. Gao, R. V. Kumar, and B. A. Glowacki, “Performance optimization of LSCF/Gd:CeO₂ composite cathodes via single-step inkjet printing infiltration”, *J. Appl. Electrochem.*, Vol. 47, No. 5, 2017, pp. 641–651, doi: <https://doi.org/10.1007/s10800-017-1066-1>.
 144. T. Y. Hill, T. L. Reitz, M. A. Rottmayer, and H. Huang, “Controlling inkjet fluid kinematics to achieve SOFC cathode micropatterns”, *ECS J. Solid State Sci. Technol.*, Vol. 4, No. 4, 2015, pp. P3015–P3019, doi: <https://doi.org/10.1149/2.0031504jss>.
 145. T. H. Lee, K. Y. Liu, F. E. Wiria, and P. C. Su, “Inkjet-printed silver and samarium-doped ceria nanocomposite cathode for low temperature solid oxide fuel cells”, *EEE/SICE International Symposium on System Integration (SII)*, 2017, pp. 83–88, doi: <https://doi.org/10.1109/SII.2017.8279193>.
 146. C. Li, H. Chen, H. Shi, M. O. Tade, and Z. Shao, “Green fabrication of composite cathode with attractive performance for solid oxide fuel cells through facile inkjet printing”, *J. Power Sources*, Vol. 273, 2015, pp. 465–471, doi: <https://doi.org/10.1016/j.jpowsour.2014.09.143>.
 147. C. C. Yu, J. D. Baik, C. H. Su, L. Fan, J. Wei, Y. C. Liao, and P. C. Su, “Inkjet-printed porous silver thin film as a cathode for a low-temperature solid oxide fuel cell”, *ACS Appl. Mater. Interfaces*, Vol. 8, No. 16, 2016, pp. 10343–10349, doi: <https://doi.org/10.1021/acsaami.6b01943>.
 148. N. Yashiro, T. Usui, and K. Kikuta, “Application of a thin intermediate cathode layer prepared by inkjet printing for SOFCs”, *J. Eur. Ceram. Soc.*, Vol. 30, No. 10, 2010, pp. 2093–2098, doi: <https://doi.org/10.1016/j.jeurceramsoc.2010.04.012>.